

	DOC:	MERIS Case 2 water ATBD 4 th reproc		
	DATE:	20150319		
	Issue:	2	Revision:	
				Page: 1 of 55

Algorithm Theoretical Bases Document (ATBD) for L2 processing of MERIS data of case 2 waters, 4th reprocessing

- draft -

Author: R. Doerffer

Distribution: P. Goryl, ESA, C. Brockmann, Brockmann-Consult, L. Bourg, ACRI, QWG

Revisions:

Issue	Date	Subject	Author
1	20140825	First issue	Doerffer
2	20150319	New Nns for AC with pressure input	Doerffer

Table of Content

1	Introduction.....	3
2	Overview.....	3
2.1	Definitions and neural networks.....	3
2.2	Flags.....	4
3	Optical Models.....	6
3.1	Bio-optical model.....	6
3.1.1	Overview.....	6
3.1.2	Phytoplankton pigment absorption.....	8
3.1.3	Absorption by Detritus and Gelbstoff.....	8
3.1.4	Scattering by particles.....	9
3.2	Ranges, frequency distribution and co-variances.....	10
3.2.1	Co-variations between the optical components.....	10
3.2.2	The algorithm to define the bio-optical model.....	13
3.2.3	Simulation of the water leaving radiance reflectance.....	14
3.3	Model of the atmosphere.....	15
3.4	Simulation of the TOSA reflectances.....	15
4	Computation of R _{tosa} from L1b data of MERIS.....	16
5	Overview of the NNs.....	17
5.1	Atmosphere NNs.....	17
5.1.1	R _{tosa} _autoNN.....	17

	DOC:	MERIS Case 2 water ATBD 4 th repro		
	DATE:	20150319		
	Issue:	2	Revision:	
				Page: 2 of 55

5.1.2Rw_invNN.....	18
5.1.3Rpath_NN.....	18
6Water NNs.....	18
6.1inverse IOP_NN.....	18
6.2Forward IOP_NN.....	19
6.3Uncertainty NN.....	19
7Optional NNs.....	20
7.1Atmospheric transmittance.....	20
7.2kd_490, kd_min and z90_max.....	20
7.3Normalisation of Rw.....	20
8Computation of chlorophyll and total suspended matter, TSM.....	20
9Computation of out-of-range, out-of-scope and uncertainties.....	21
9.1Out-of-range flags.....	21
9.2Out-of-scope reflectances and flags.....	21
9.3Uncertainties of IOPs.....	22
10Validation of the algorithms.....	24
10.1Validation using data of the Helgoland transects.....	24
10.1.1Transect C18 20050420.....	24
10.1.2Transect C23, 20050901.....	27
10.1.3Transect C24 20051006.....	29
10.1.4Transect C25, 20051013.....	31
10.1.5Transect C26, 20060508.....	33
10.1.6Transect C27, 20060511.....	35
10.1.7Transect C28, 20060612.....	37
10.1.8Transect C29, 20060704.....	39
10.1.9Transect C32, 20060726.....	41
10.1.10Summary and conclusions from Helgoland transects.....	42
10.2Validation using MERMAID data.....	43
10.2.1Retrieval of Rw.....	43
10.2.2Validation of chlorophyll data.....	46
10.2.3Validation using HPLC total data.....	47
10.2.4Test using the fluorometric chlorophyll data.....	48
10.2.5Summary and conclusions from the MERMAID test.....	50
10.3Test of the case 2 water procedure for high altitude inland waters.....	50
10.4Sun glint and high reflectance test.....	51
11Summary and Conclusions.....	53
12Acronyms.....	53
13References.....	55

	DOC:	MERIS Case 2 water ATBD 4 th reproc		
	DATE:	20150319		
	Issue:	2	Revision:	

1 Introduction

This document describes the theoretical background and the design of the case water algorithms for the 4th reprocessing of MERIS data. It includes a description of the atmospheric and bio-optical model, the architecture of the neural networks and other routines and the results of performance tests using a breadboard processor.

The algorithms and corresponding neural networks are split into 2 parts:

- (1) retrieval of water leaving reflectance R_w from Top of Atmosphere (TOA) reflectances R_{toa} and
- (2) retrieval of inherent optical properties (IOPs) from water leaving reflectances R_w .

The second part can also be used in conjunction with the standard atmospheric correction.

The algorithms and corresponding neural networks are complemented with procedures to identify spectra, which are out of scope of the algorithms, and determine the uncertainties of the IOPs.

Changes with respect to version 1

The new version (2, 20150319) includes neural networks for the atmospheric correction with the surface pressure as input, so that the pressure correction part for Rayleigh scattering in the TOA-TOSA conversion can be omitted.

Furthermore included are a NN to compute the upward and downward directed transmittances through the atmosphere, the downwelling irradiance attenuation kd_{490} and k_{min} , and a NN to compute the normalized water reflectance.

2 Overview

2.1 Definitions and neural networks

An overview about all components is given in Fig. 1. Here all boxes with light yellow are optional, should be included in ODESA, but do not lead to standard products. The optional products have a glue-grey color.

The chain of networks starts from top of standard atmosphere reflectances,

$$R_{tosa} = L_{tosa}/E_{dtosa} * PI$$

Top of standard atmosphere (TOSA) is defined as the atmosphere with a ground pressure of 1013.2 hPa and without any absorbing gases (also no ozone). L_{tosa} and E_{dtosa} are computed from MERIS L1 data (L_{toa} and E_{dtoa}) using a preprocessor, because the NNs are trained for these TOSA conditions. Furthermore, R_{tosa} is based on the nominal wavelengths of MERIS; thus, it is expected that the “smile correction” is also included in the preprocessing step.

The case 2 water procedure consists of the following 9 NNs:

- aaNN: for testing if R_{tosa} is within the scope of the training data,
- atmospheric correction NNs: for computing (1) water reflectance R_w , (2) path radiance reflectance R_{path} and (3) the downwelling transmittance td and the upward directed transmittance tu from R_{tosa} ,

	DOC:	MERIS Case 2 water ATBD 4 th reproc		
	DATE:	20150319		
	Issue:	2	Revision:	

- normalisation NN: for computing the fully normalised R_{wn} , i.e. with the sun in zenith and the nadir viewing direction,
- water IOPs NN: for computing IOPs of water from R_w
- water reflectance NN: for computing R_w from IOPs
- uncertainty NN: for computing the standard deviation of the log of IOPs
- kd NN: for computing the downwelling irradiance attenuation coefficient for 490 nm (kd490) and for the mean of the 3 spectral MERIS bands with the lowest kd (kadmin). Kadmin can be converted into the signal depth z_{90} , which is an estimate of the depth from which 90% of the upwelling directed radiance just below the surface stems from: $z_{90} = 1/k_{admin}$.

To be consistent with the other variables in MERIS processing all reflectances are defined as

$$R = L / Ed * \pi$$

Note: all NNs (except the IOP uncertainties NN) have the sun and viewing angles as well as the water temperature and salinity as input. The atmospheric correction Nns have also the surface pressure as input.

The viewing angle for the atmosphere NNs is given as x, y, z coordinates:

$$x = \sin(\text{view_zeni}) * \cos(\text{azi_diff}); y = \sin(\text{view_zeni}) * \sin(\text{azi_diff}); z = \cos(\text{view_zeni})$$

view_zeni is the viewing zenith angle and azi_diff is the difference between the azimuth of the sun and viewing angle in the range 0-180 deg, where at 180 deg MERIS is looking in direction of the sun (sun glint condition).

$$\text{azi_diff} = \text{acos}(\cos(\text{view_azi} - \text{sun_azi})).$$

2.2 Flags

The check if R_{tosa} is within the scope of the training data is performed using the auto-associative NN (aaNN). If the difference between the input and output R_{tosa} surmounts a certain threshold a warning flag is set.

A further test is performed by using the output of the NN for computing the path radiance.

Out of scope conditions of the water leaving reflectance spectrum (R_w) is performed by comparing R_w with the output of the forward NN (IOPforNN), which computes R_w from the result of the inverse IOP NN (IOPinvNN) and sets a the flag if the difference surmounts a given threshold.

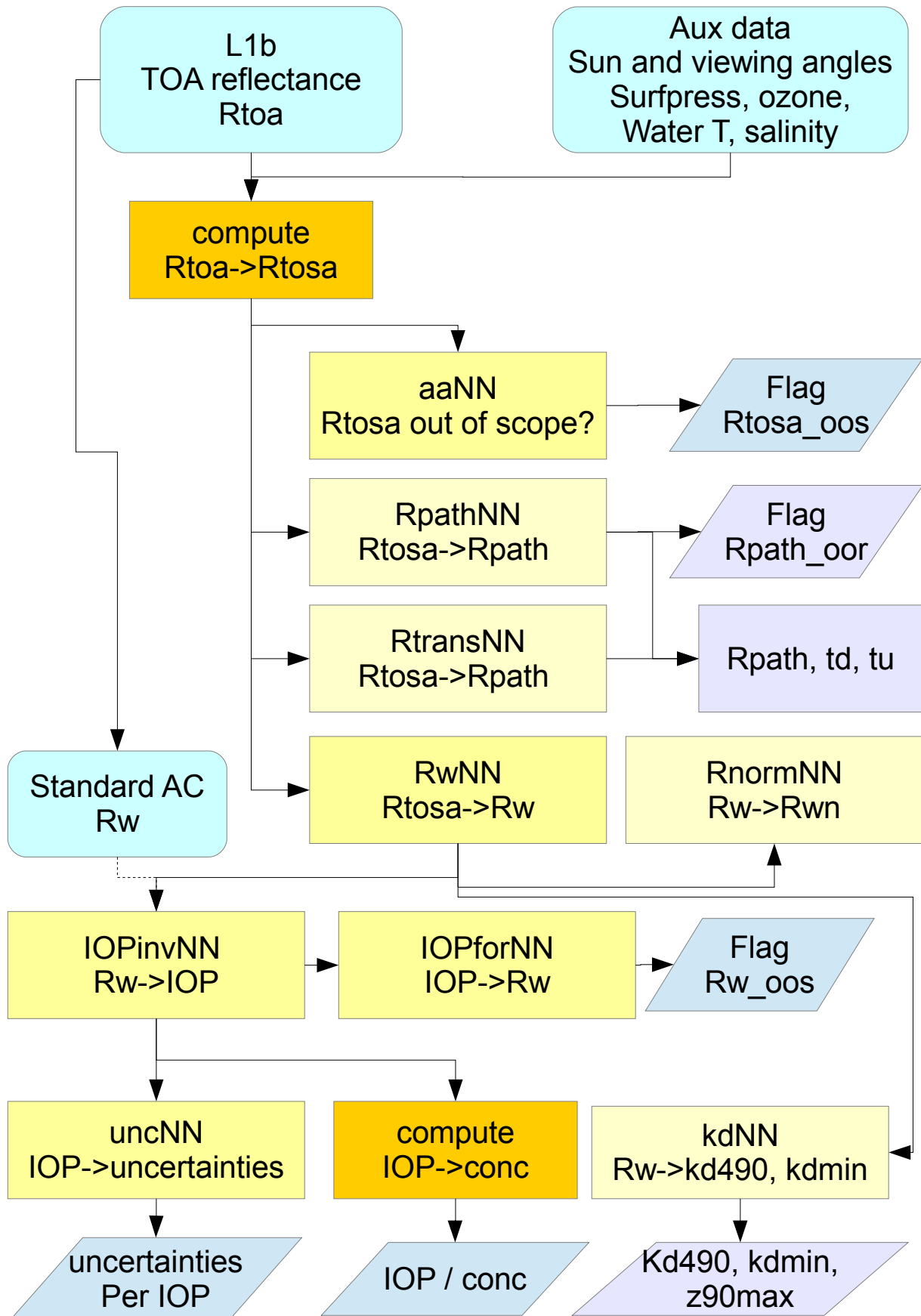


Fig. 1: Outline of the L2 case2 water processing

 BROCKMANN CONSULT	DOC:	MERIS Case 2 water ATBD 4 th reproc		
	DATE:	20150319		
	Issue:	2	Revision:	

3 Optical Models

The case 2 water algorithms of MERIS are based on optical models of the atmosphere and the water and on radiative transfer simulations, which establish the relationship between concentrations and optical properties of hydrosols and aerosols and reflectances at the water surface and at TOSA and which are used to compute the data for training of the neural networks.

Parameters of these models determine also the scope of the algorithms;

- number, kind and inherent optical properties (IOP) of the optical components, which represent the water constituents
- relationship between mass concentration and IOPs
- concentration range, frequency distribution and co-variances between the components
- environment of the model: vertical distribution, sea surface roughness, effects of wind, temperature and salinity, range of solar and viewing angles, atmospheric pressure.

All of these parameters will be described in the following sections.

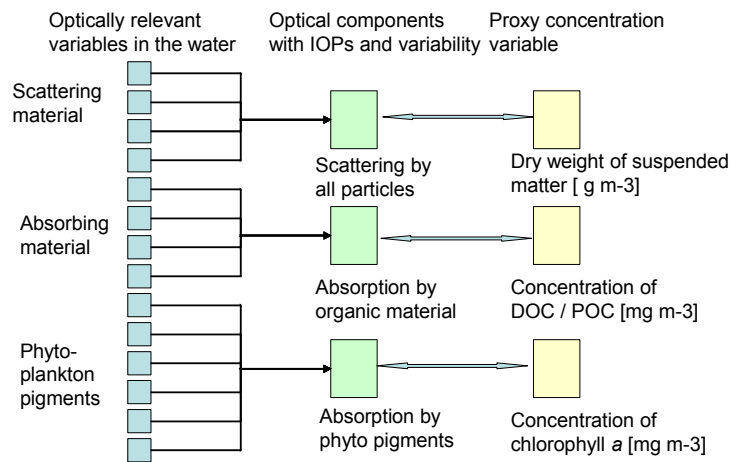
3.1 *Bio-optical model*

3.1.1 *Overview*

The spectral optical properties, i.e. absorption $a(\lambda)$ and scattering $b(\lambda)$, of sea water and inland waters are determined by a large number of different water constituents. These include different kinds of mineral particles, different species of phytoplankton, bacteria and protozoa, detritus, i.e. decomposed remaining of organisms, macro-molecules such as different kind of humic substances.

All of these constituents contribute more or less and spectrally dependent to the reflectance spectrum. Since it is impossible to determine all of these constituents inversely from a reflectance spectrum, it is necessary to reduce this manifold of variables to a few optical components, which are sufficient to describe the variability of reflectance spectra of a coastal region or the global ocean.

	DOC:	MERIS Case 2 water ATBD 4 th reproc		
	DATE:	20150319		
	Issue:	2	Revision:	



In case 1 water, by definition, there is only 1 optical component necessary to describe the variability of reflectance spectra. In case of the open ocean it is a mean phytoplankton community, of which mainly its pigments determine the absorption spectrum.

For case 2 water, by definition, more than one component have to be used to describe the variability of the reflectance spectra.

For the presented MERIS case 2 water algorithms 5 optical components have been defined:

- absorption by phytoplankton pigments (*apig*)
- absorption by detritus (*ad*)
- absorption by yellow substances (gelbstoff) (*ag*)
- scattering by mean coastal particles (*bp*)
- scattering by white particles (*bw*)

The absorption or scattering spectra of *ad* and *ag* and of *bp* and *bw* respectively are regarded as the lower and upper end of the natural range of the spectral shape of only 1 component so that finally only 3 components are provided as products to the user: *apig*, *adg*, *btsm*.

Apig is converted into chlorophyll concentration and *btsm* in TSM dry weight, while the product of *adg* remains as an absorption coefficient. All spectral properties are normalized at 443 nm, the absorption or scattering coefficients at this wavelength are the output of the IOP neural network.

Basis for this bio-optical model is the NOMAD data set of NASA(cite xx), which has been compiled for the development of algorithms from sites all over the global ocean. For the case 2 water bio-optical model it has been extended with respect to higher concentrations from measurements in the North and Baltic Sea and on the bases of the Coastcolour data set. Coastcolour was an ESA funded international research project to exploit the potential of MERIS full resolution data of coastal sites all over the world. Within the frame of this project in situ data (optical properties, concentrations) were provided by the participants and compiled in a central data base.

	DOC:	MERIS Case 2 water ATBD 4 th reproc		
	DATE:	20150319		
	Issue:	2	Revision:	Page: 8 of 55

3.1.2 Phytoplankton pigment absorption

A mean phytoplankton absorption spectrum was derived from NOMAD data set. For this purpose pigment absorption was calculated as the difference $apig = ap - ad$, where ap is the absorption by particles, and ad by detritus. All absorptions were normalized to the absorption at 443 nm (Fig. 3). Then the mean at each of the available 20 spectral bands was calculated. This mean spectrum was finally interpolated to get the spectral bands of MERIS (s. Table 1).

Band / λ	1/412	2/443	3/489	4/510	5/560	6/620	7/665	8/681	9/708
rel. a	0.95	1.0	0.64	0.42	0.15	0.124	0.242	0.247	0.098

Table 1: Relative absorption of phytoplankton pigments

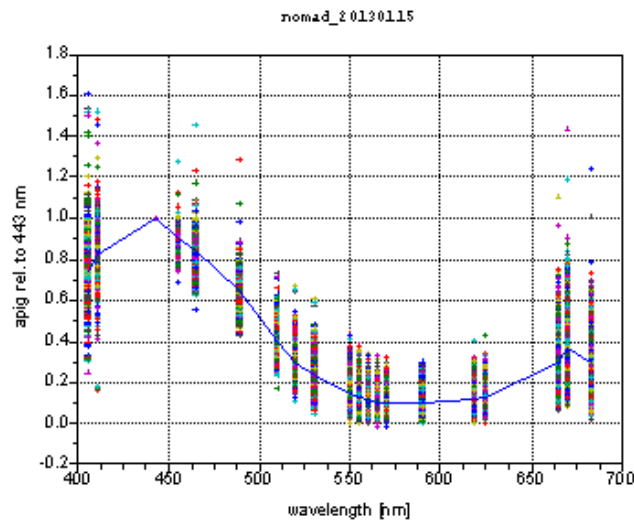


Fig. 3: Variability of the pigment absorption coefficient relative to 443 nm and the mean absorption spectrum from the NOMAD data set

Regarding the sunlight induced fluorescence of phytoplankton s. chapter 3.2.3.

3.1.3 Absorption by Detritus and Gelbstoff

The absorption spectra of detritus, ad , and gelbstoff, ag , are parameterized by

$$ad(\lambda) = ad_{443} * \exp(-ex_{ad} * (\lambda - 443))$$

$$ag(\lambda) = ag_{443} * \exp(-ex_{ag} * (\lambda - 443))$$

The exponents ex_{ad} and ex_{ag} have been determined from the NOMAD data set. Since both have a large overlap the upper value (95% percentile) of ex_{ag} and the lower end (5% percentile) of ex_{ad} were used to bracket most of the absorption spectra of ad and ag .

$$ex_{ag} = 0.025$$

	DOC:	MERIS Case 2 water ATBD 4 th reproc		
	DATE:	20150319		
	Issue:	2	Revision:	Page: 9 of 55

$$ex_{ad} = 0.0074$$

The frequency distribution of both exponents are shown in Fig. 4 and Fig. 5

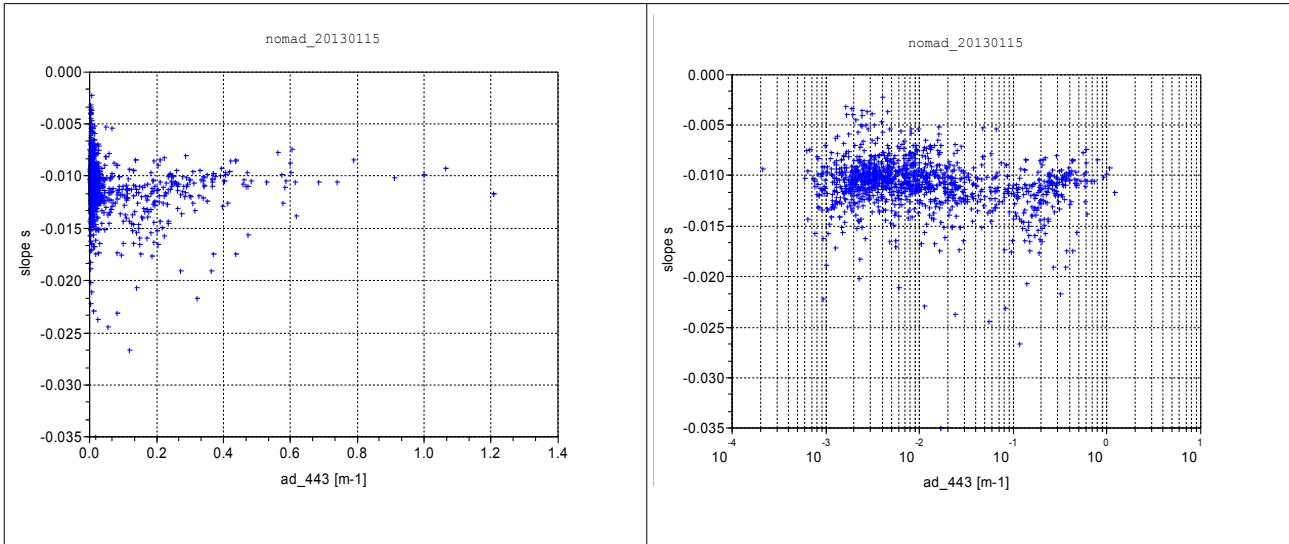


Fig. 4: Spectral exponent of detritus absorption, ad , as a function of the detritus absorption coefficients of the NOMAD data set, left on linear, right on log scale

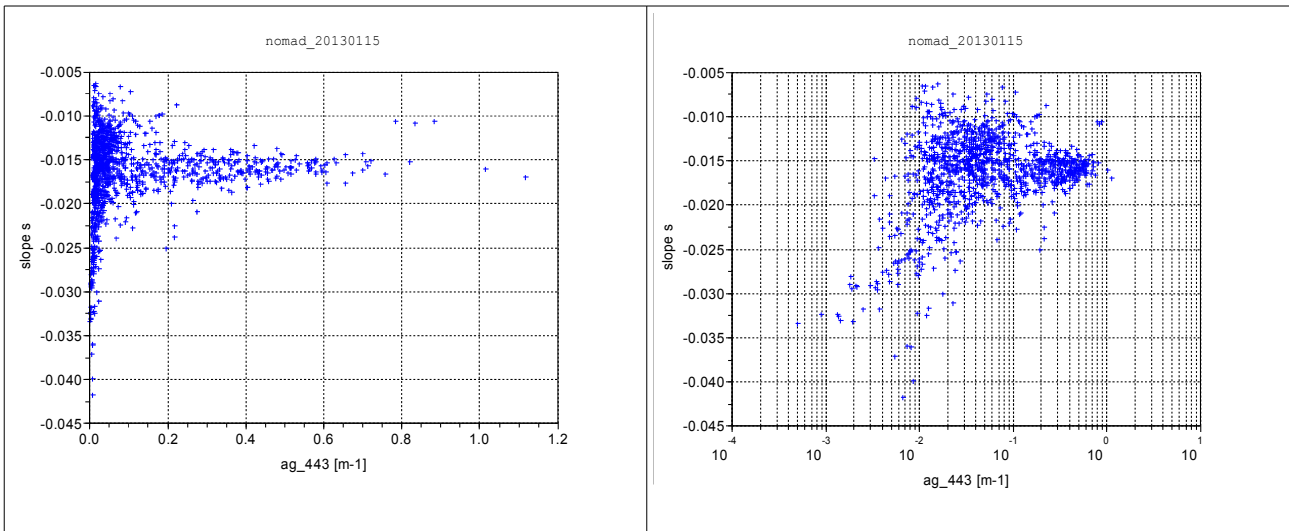


Fig. 5 Spectral exponent of gelbstoff absorption, ag , as a function of the gelbstoff absorption coefficients of the NOMAD data set, left on linear, right on log scale

3.1.4 Scattering by particles

The scattering by particles is parametrized in a similar way by two exponents, which bracket the scattering coefficients of the broad range of particles in waters. One end is represented by white particles, i.e. $ex_{bw} = 0$, to cover e.g. coccolithophorides and foam on the water, while the other end with an exponent of 1.87 is represented by small particles. It has been derived from the 95% percentile of the backscattering coefficients of the NOMAD data (s. Fig. 6).

	DOC:	MERIS Case 2 water ATBD 4 th reproc		
	DATE:	20150319		
	Issue:	2	Revision:	
				Page: 10 of 55

$$bp(\lambda) = ((443.0/\lambda)**ex_bp) * conc_bpart$$

$$bw(\lambda) = ((443.0/\lambda)**ex_bw) * conc_bwit$$

$ex_bp = 1.87$ // with $Bb = 0.018$ from the Petzold phase function
 $ex_bw = 0.0$ // with $Bb = 0.008$

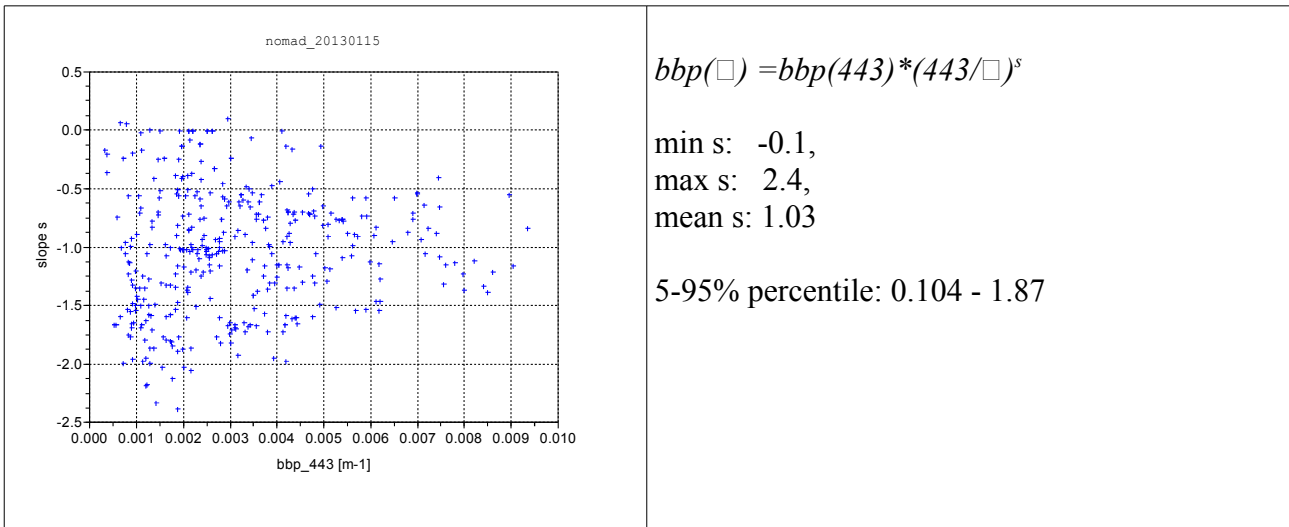


Fig. 6: Spectral exponent of particle backscattering, s , as a function of the backscattering coefficient, NOMAD data set

Only one scattering phase function was used for both scattering components, which is the Petzold "average particle" phase function, as listed in Mobley, xx, Table 3.10, and which is included in Hydrolight as "avgpart.dpf".

3.2 Ranges, frequency distribution and co-variances

For the successful training and application of neural networks it is not only necessary to define the absorption and scattering properties, but also the frequency distribution and the co-variances of the components. The bio-optical model should be as tight as possible to the true conditions with respect to these parameters, but should also be open to natural conditions, which were not included in the data set, from which the bio-optical was derived.

These parameters were first determined for the NOMAD data set. Goal was that the bio-optical model should cover at least all of these parameters of the NOMAD data but also those of higher concentrations such as e.g. present in estuaries.

3.2.1 Co-variations between the optical components

The co-variations between all optical components of the NOMAD data set ($apig$, ad , ag , ap and between ap and bp) have been analyzed and used for defining the bio-optical model.

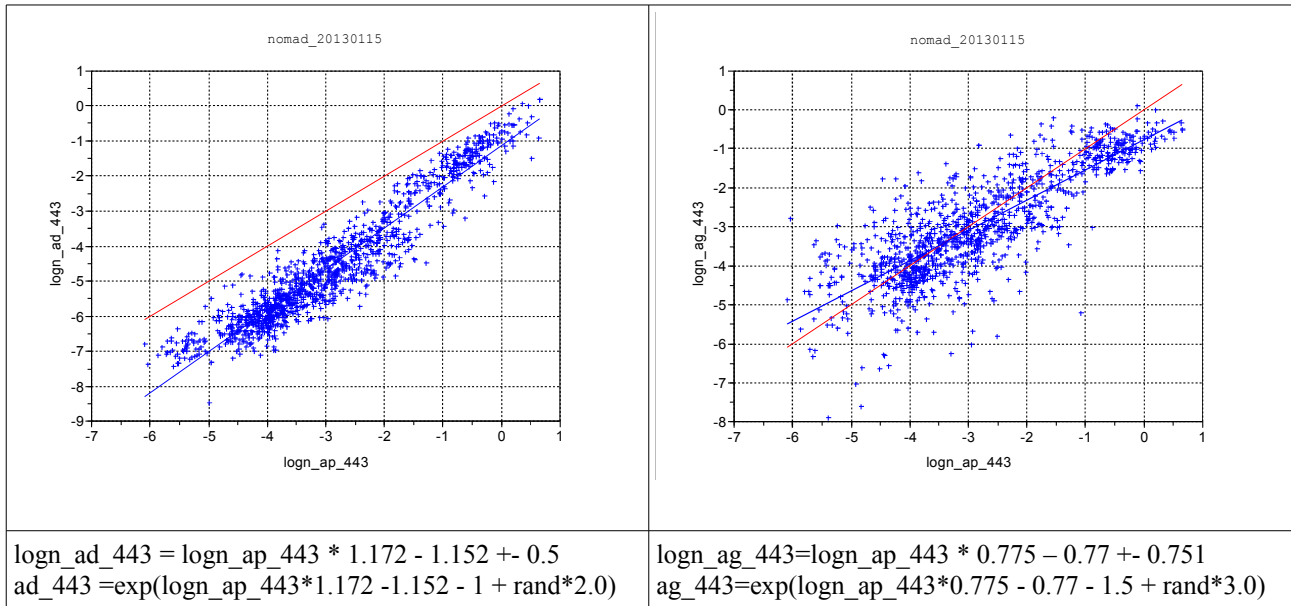


Fig. 7: Relationship between detritus and total particle absorption (left) and between gelbstoff and total particle absorption (right) with the corresponding regression coefficients and the formulation for the bio-optical model

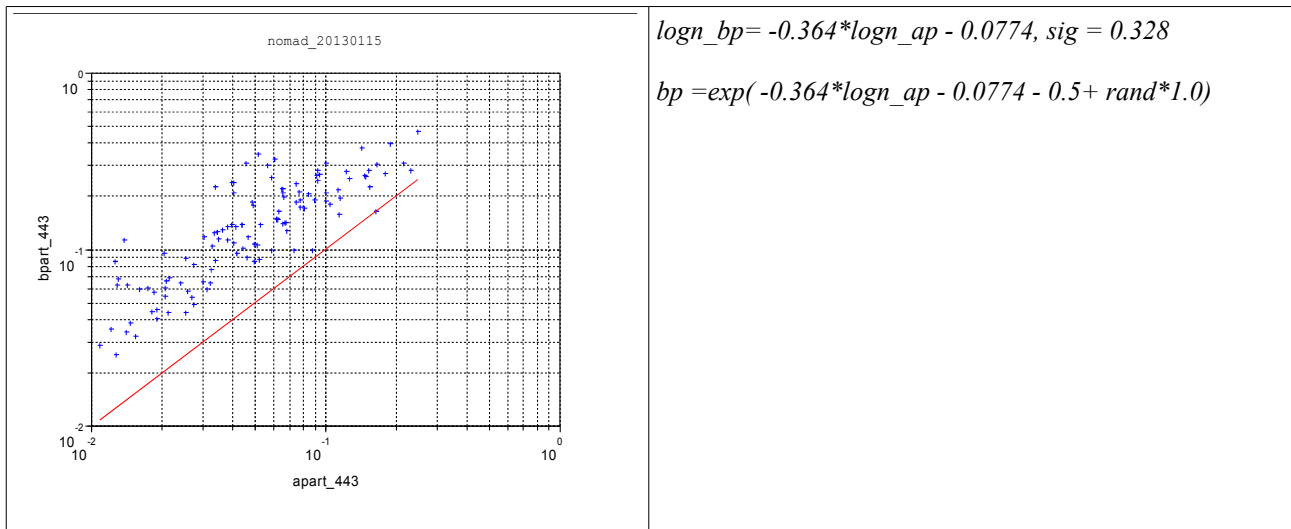


Fig. 8: Relationship between the backscattering and absorption coefficient at 443 nm of the NOMAD data set and the corresponding formulation for the bio-optical model

The relationships between the IOP components as defined in the bio-optical have then be compared with the NOMAD data.

	DOC:	MERIS Case 2 water ATBD 4 th reproc		
	DATE:	20150319		
	Issue:	2	Revision:	

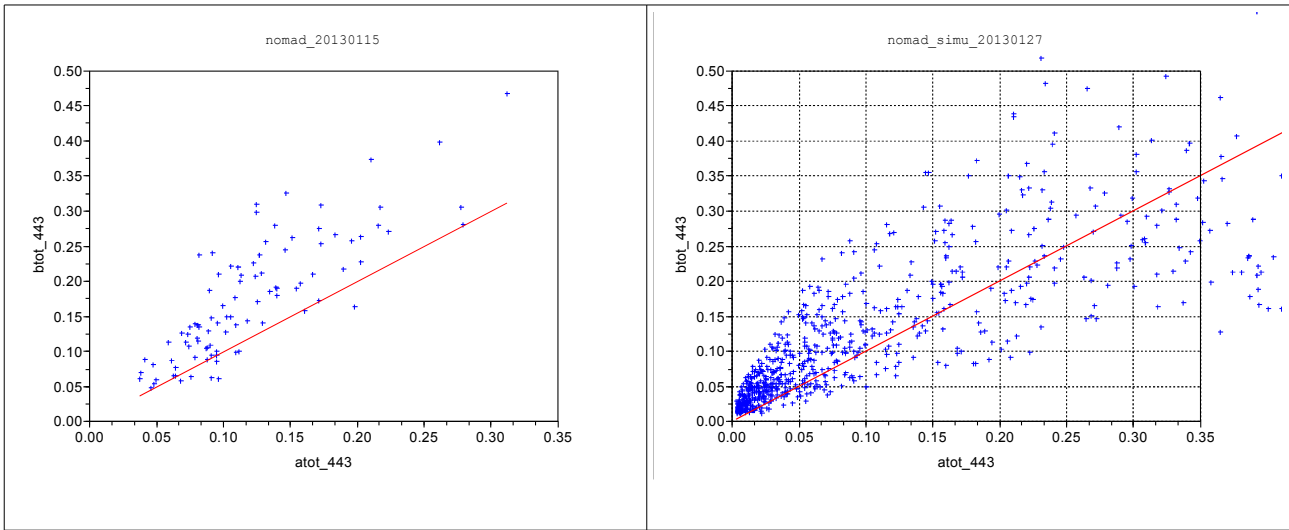


Fig. 9: Relationship between particle absorption and backscattering, left NOMAD, right simulated

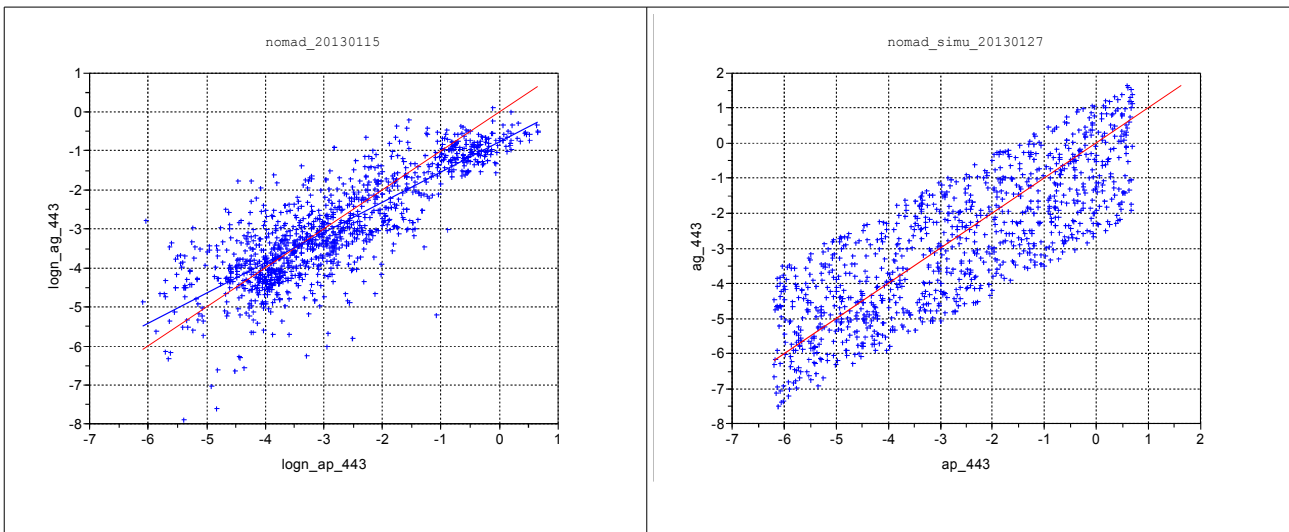


Fig. 10: Relationship between particle and gelbstoff absorption, left NOMAD, right simulated

	DOC:	MERIS Case 2 water ATBD 4 th reproc		
	DATE:	20150319		
	Issue:	2	Revision:	Page: 13 of 55

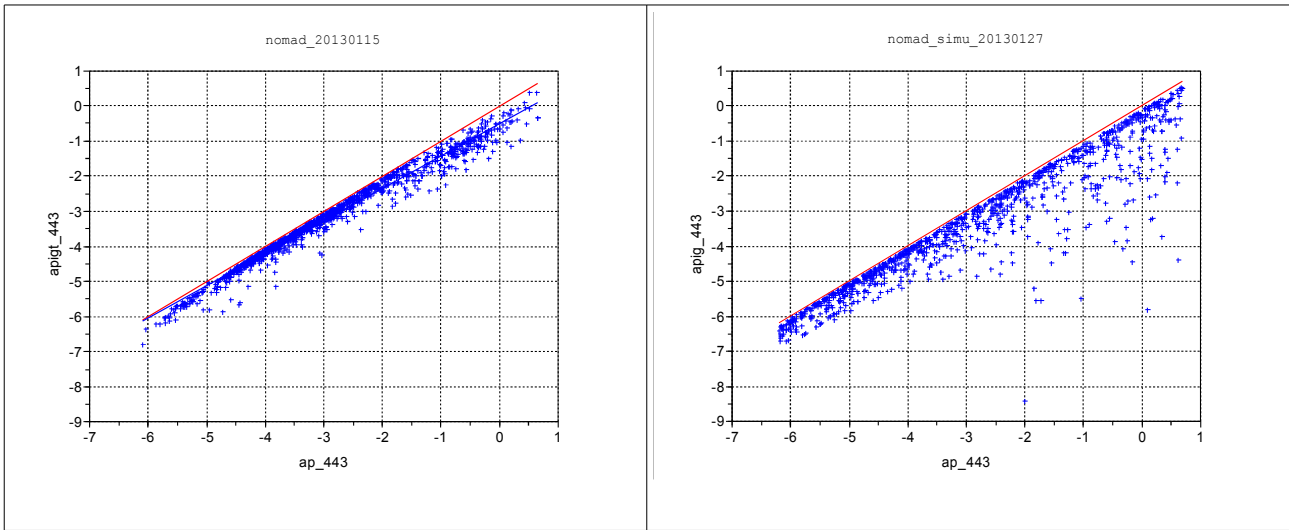


Fig. 11: Relationship between particle and pigment absorption, left NOMAD, right simulated

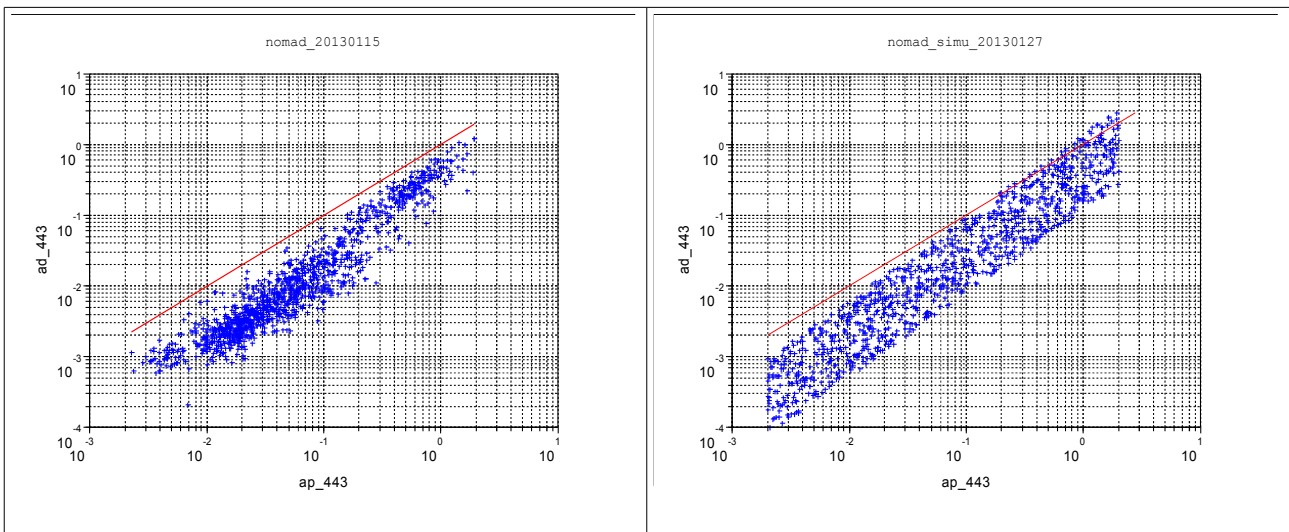


Fig. 12: Relationship between particle and detritus absorption, left NOMAD, right simulated

3.2.2 The algorithm to define the bio-optical model

The ranges, frequency distribution and co-variances (as described above) have been used to set up a procedure, which is called for each simulated case and which computes the IOPs for this case randomly within the limits of the bio-optical model. In an additional step the phytoplankton concentration (in the form of *apig*) is limited due to the attenuation of all other substances and the sun zenith angle.

The procedure starts alternately from case to case either with the total absorption or total scattering. A randomly selected value within the limits is taken from the logarithmic scale and then the corresponding scattering or absorption coefficient is selected also randomly but constraint by the limits given by the co-variance. In the next step the absorption coefficient is split into *apig*, *ad* and

	DOC:	MERIS Case 2 water ATBD 4 th reproc		
	DATE:	20150319		
	Issue:	2	Revision:	Page: 14 of 55

ag also randomly but with respect to the range of co-variances. This splitting starts also case by case alternatively with $apig$, ad or ag . The same procedure is performed for splitting the scattering coefficient b into bp and bw . By this alternation the co-variances start always from a different value of a or b and from $apig$, ad or ag and from bp or bw .

The pure water IOPs are also computed case by case with randomly selected temperature and salinity.

All parameters are summarized in Table xx.

3.2.3 Simulation of the water leaving radiance reflectance

The water leaving radiance reflectances $RL(\lambda, \theta_v, \varphi) = L_w(\lambda, \theta_v, \varphi)/E_d(\lambda, \theta_s)$ are simulated using the Hydrolight 5.2 radiative transfer code with some modification.

One subroutine was added for computing the absorption and scattering coefficients of the 5 components (s. above) and change these randomly together with the sun zenith angle and the wind speed. Also water temperature and salinity are changed randomly for computing pure water absorption and scattering coefficients as well as the refractive index.

For all water constituents a vertically homogeneous distribution in an infinite deep water with a wind dependent rough surface and a variable sun zenith angle is assumed.

Inelastic scattering (Fluorescence, Raman scattering) is not used in Hydrolight, but the sunlight stimulated fluorescence of phytoplankton is computed with a two-flow model using a fluorescence efficiency of 3% of the energy, which is absorbed by $apig$, and emitted spectrally at 685 nm using a Gaussian-type distribution with a sigma of 10.4 nm. The contribution by fluorescence is stored separately as Rwf so that it can be added optionally to the reflectance for the NN training run.

To avoid overshooting of the NN between the training points randomly selected uncertainties of up to 5% using a normal distribution are added to the simulated reflectance data independently for each spectral band.

To check if the simulated water leaving reflectances R_w of this bio-optical model cover measured reflectances, they are compared with R_w_{443} and R_w_{560} of NOMAD and MERMAID in the form of a scatter plot.

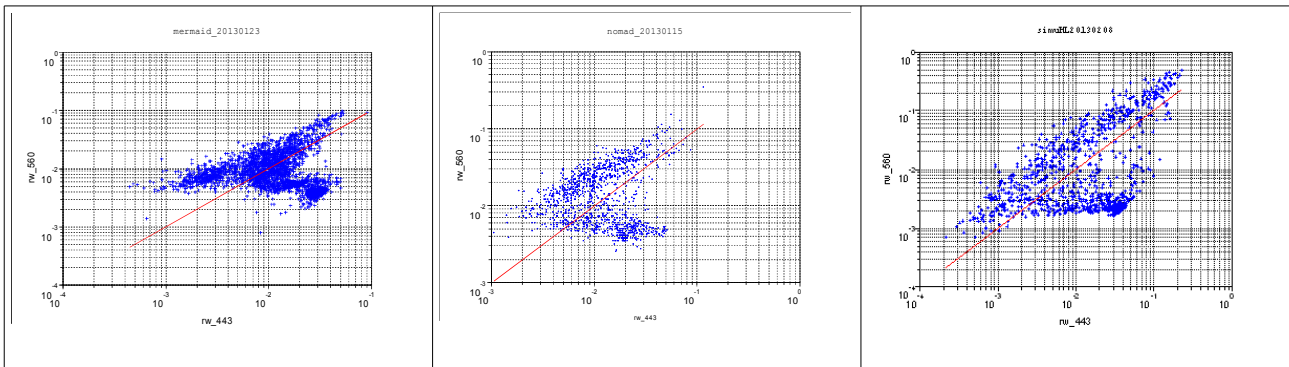


Fig. 13: Scatter plot of the reflectance at 560 nm versus 443 nm of MERMAID, NOMAD and of the simulated data, note the different scales

	DOC:	MERIS Case 2 water ATBD 4 th reproc		
	DATE:	20150319		
	Issue:	2	Revision:	Page: 15 of 55

3.3 Model of the atmosphere

The model of the atmosphere has been developed by R. Santer and R. Zagolski for the Coastcolour project (based on Zagolski et al, 2007, Aznay & Santer, 2009). It is based on an analysis of AERONET data of coastal sites. These data were used for simulating path radiances and transmittances for various aerosol types, surface pressures and sun elevations, which are stored in a data base. The simulation is based on Lenoble et al, 2007. A program is then used to extract and interpolate the requested data for a certain sun zenith angle, surface pressure, aerosol optical thickness, angstrom coefficient and wind speed. This program was complemented to compute the temperature and salinity wavelength dependent refractive index of water for simulating the specular reflectance of direct sun light (sun-glint) and sky light.

3.4 Simulation of the TOSA reflectances

The TOSA reflectances are computed by combining the atmosphere model with the forwardNN for water and the phytoplankton fluorescence model.

For each simulation run (case) a random value of the following parameters is selected from a uniform distribution:

sun zenith angle: 0 -75 deg

view zenith angles: 0 – 60 deg

view azimuth angle: 0 -180 deg

surface pressure: 800 – 10140 hPa

aerosol optical thickness (aot at 550 nm): 0.0 – 0.8

angstrom coefficient: 0.0 – 2.5

wind speed: 0 – 10 m s⁻¹

water temperature: 0 – 36 deg C

salinity: 0 – 43

For the corresponding sun and viewing angle and temperature and salinity the water leaving irradiance reflectance is computed using the forward NN. Here the randomly chosen variables are the 5 IOPs. Values of these 5 IOPs are selected randomly according to the frequency distribution as described in chapter 3.1.

Also the contribution by phytoplankton fluorescence is computed using the two-flow model and the values of the 5 IOPs.

The water reflectances as well as the fluorescence is transported to TOSA using the up and downward transmittances, t_u and t_d , for the corresponding sun and viewing angles from the atmosphere model.

For each case of the atmosphere 9 randomly selected cases of IOPs are used. Finally a randomly selected uncertainty of 1% is added to the TOSA reflectances for each band independently.

Alltogether 1.35 million TOSA cases are generated for training of the atmosphere NNs, i.e. for determining R_w , R_{path} , t_d and t_u from R_{tosa} as well as the aaNN for detecting out of scope spectra.

	DOC:	MERIS Case 2 water ATBD 4 th reproc		
	DATE:	20150319		
	Issue:	2	Revision:	

4 Computation of *R_{toa}* from L1b data of MERIS

The neural networks for the atmospheric correction are trained for a standard atmosphere, which is defined here as an atmosphere without any absorbing gases including ozone. This requires that the L1b data of MERIS have to be converted for these TOSA conditions into *R_{toa}* by using the actual ozone concentration, which is provided in the auxiliary data of MERIS. Furthermore, the 708 nm band of MERIS has to be corrected for the influence of water vapour by using the information from the MERIS water vapour bands 14 and 15. Another task, which has to be performed in the preprocessor is the “smile effect” correction, but this will be performed outside the algorithms of this ATBD.

Note that in MEGS / ODESA also the gas correction will be performed outside the procedures described here.

The following procedure is presented in Scilab code notation:

Start is the computation of the top of atmosphere (TOA) reflectance *R_{toa}*

$$R_{toa} = L_{toa} / (solflux * \cos_{sun}) * \pi;$$

with *L_{toa}*, the top of atmosphere radiance, *solflux*, the solar flux at TOA, *cos_{sun}*, the cosine of the sun zenith angle, all as present in MERIS L1b products and multiplied by PI to get formally the dimensionless irradiance reflectance.

Reflectance of band 9 (708 nm) is corrected for the influence of water vapour by using the reflectance at band 15 (900 nm) and 14 (885 nm) according to the standard water vapour correction of MERIS as implemented in MEGS.

$$X2 = R_{toa}(15) / R_{toa}(14);$$

$$trans_{708} = h2o_corpoly(1) + h2o_corpoly(2) * X2 + h2o_corpoly(3) * X2^2 + h2o_corpoly(4) * X2^3;$$

with *h2o_corpoly* the polynomial, with the following coefficients:

$$h2o_cor_poly = [0.3832989, 1.6527957, -1.5635101, 0.5311913];$$

$$R_{toa}(9) = R_{toa}(9) / trans_{708};$$

The absorption by ozone of the downwelling irradiance and the upwelling radiance in the direction of the sensor is computed using the ozone column content of the atmosphere in Dobson units as included in the auxiliary data of the L1b product and the ozone absorption coefficients [cm⁻¹] for the MERIS bands:

band	1	2	3	4	5	6	7	8	9	10	12	13
A [cm ⁻¹]	8.20E-4	2.82E-3	2.08E-2	3.96E-2	1.02E-1	1.06E-1	5.31E-2	3.55E-2	1.90E-2	8.38E-3	7.20E-4	0.0

Table 2: Ozone absorption coefficients, *a_{ozone}* [cm⁻¹], for MERIS bands 1-10, 13, 13

The transmittance is then calculated as

$$trans_{ozone} = \exp(-(a_{ozone} * c_{oz} / 1000) / \cos_{sun} + a_{ozone} * c_{oz} / 1000) / \cos_{view}$$

with *a_{ozone}*, the absorption coefficient of ozone per [cm⁻¹] and *c_{oz}*, the concentration of ozone in Dobson units.

$$R_{toa} = R_{toa_h20} / trans_{ozone};$$

	DOC:	MERIS Case 2 water ATBD 4 th reproc		
	DATE:	20150319		
	Issue:	2	Revision:	Page: 17 of 55

5 Overview of the NNs.

The neural networks are trained using a *backpropagation-of-error* algorithm. The training and application programs were developed by H. Schiller at HZG. The training program is based on the Stuttgart Neural Network training program (SNNS).

The full set of all 9 NNs is based on the same bio-optical water model, i.e. it provides also the boundary for the atmosphere NNs.

The training data set for the water comprises 150 000 different cases, each for 7 different angles, all of which are randomly selected from the range as described above in chapter xx. From these 1050000 cases 20% are randomly separated and used for testing during the training run to ensure that the overall error of the NN of the training and test data sub sets is the same (within 1%) to prove if overtraining has occurred, which would reduce the interpolation performance of the NN.

For the atmosphere NNs (*Rpath*, *td*, *tu*, *aaNN*) also 150 000 cases are simulated for randomly selected aerosol optical thickness, angstrom coefficient, wind speed and sun and observation angles. For each of these cases 9 different and randomly selected water cases are simulated using the forward water NN. The water reflectance is then multiplied for the corresponding angles with the downward and upward transmittances to get the TOSA reflectance together with the path reflectance and water reflectance.

$$R_{tosa} = R_{path} + td*tu*R_w$$

All angles (sun zenith angle, *sun_zeni*, viewing zenith angle, *view_zeni*, and difference between sun and viewing azimuth angle, *azi_diff*, are given in degrees. Azimuth difference *azi_diff* is defined as for MERIS, i.e. above water the sun glint would be seen under an azimuth difference of 180 deg. For the atmosphere NNs the viewing angle together with the azimuth difference is given in x, y, z coordinates to reduce artefacts around the nadir looking angle, which would come in MERIS products from the interpolated azimuth differences near the nadir.

5.1 Atmosphere NNs

Note: For all atmosphere NNs 12 bands are used: rw412 - rw753, rw778, rw865

All atmosphere NNs have 19 inputs:

- sun zenith angle
- x,y,z viewing direction
- water temperature
- salinity
- surface atmosphere pressure
- *log_Rtosa*, 12 MERIS bands (412, 443, 489, 510, 560, 620, 665, 681, 709, 754, 779, 865 nm)

5.1.1 *Rtosa_autoNN*

This NN is used to check if *Rtosa*, which is derived from Rtoa in the preprocessing step, is within the scope of the training data set.

Input and output of the NN are *Rtosa* reflectances at all 12 spectral bands. Further inputs are the sun

	DOC:	MERIS Case 2 water ATBD 4 th reproc		
	DATE:	20150319		
	Issue:	2	Revision:	
				Page: 18 of 55

zenith angle, the viewing angle in the form of x, y, z coordinates, the temperature and salinity and the surface pressure.

First a test is performed if any of the input variables is out of the range of the NN.

Core of the out-of-scope algorithm is the relative deviation between each band of the input and output R_{tosa} , which is expressed as the ratio. The maximum deviation of all bands is then compared with a threshold (tbd) to trigger the out-of-scope flag.

5.1.2 R_w_{invNN}

This network is used to determine water leaving reflectances, R_w .

$R_w = L_w / E_{dboa} * \pi$, with L_w the water leaving radiance and E_{dboa} the downwelling irradiance at the bottom of atmosphere. Output are \log_R_w in all 12 bands.

5.1.3 R_{path_NN}

This NN is used to compute the path radiance, which includes the specular reflectance of the water surface (sky and sun glint). It is used to flag clouds, which were not captured by the cloud detection algorithm.

Path radiance reflectance is $R_{path} = L_{path} / E_{dtosa} * \pi$, with L_{path} the path radiance and E_{dtosa} , the downwelling irradiance top of standard atmosphere. Output are \log_R_{path} in all 12 bands

6 Water NNs

The algorithms to retrieve the water IOPs consists of 3 neural networks.

Note: For all water NNs only 10 bands are used: rw412 - rw754

6.1 inverse IOP_NN

This NN is used to determine 5 IOPs from water reflectances R_w , with $R_w = L_w / E_{d_boa} * \pi$, all at a wavelength of 443 nm and per meter [m⁻¹].

- \log_conc_apig is the natural log of the absorption coefficient of phytoplankton pigments,
- \log_conc_adet is the natural log of the absorption coefficient of detritus
- \log_conc_agelb is the natural log of the absorption coefficient of gelbstoff, i.e. absorption coefficient of all water constituents, which pass a filter with a pore size of 0.2 μm .
- \log_conc_bspm is the total scattering coefficient b of suspended matter
- \log_conc_bwit is the total scattering coefficient b of white scatterers, e.g. of coccolithophorides, bubbles and foam.

the net has 15 inputs:

- *input 1 is sun_zeni*
- *input 2 is view_zeni*
- *input 3 is azi_diff*
- *input 4 is temperature*

	DOC:	MERIS Case 2 water ATBD 4 th reproc		
	DATE:	20150319		
	Issue:	2	Revision:	
				Page: 19 of 55

- *input 5 is salinity*
 - *input 6 - 15 are: log_rw_412, _443, _489, _510, _560, _620, _665, _681, _709, log_rw_754*
- the net has 5 outputs:
- *output 1 is log_conc_apig*
 - *output 2 is log_conc_adet*
 - *output 3 is log_conc_agelb*
 - *output 4 is log_conc_bspm*
 - *output 5 is log_conc_bwit*

6.2 Forward IOP_NN

This NN is used to compute the water reflectances from the IOPs, which are derived from the inverse NN. By comparing R_w' with the input R_w , spectra are identified, which are out of scope of the training range.

the net has 10 inputs:

- *input 1 is sun_zeni*
- *input 2 is view_zeni*
- *input 3 is azi_diff*
- *input 4 is temperature*
- *input 5 is salinity*
- *input 6 is log_conc_apig*
- *input 7 is log_conc_adet*
- *input 8 is log_conc_agelb*
- *input 9 is log_conc_bspm*
- *input 10 is log_conc_bwit*

the net has 10 outputs:

output 1 - 10 are log_rw_400, _412, _443, _489, _510, _560, _620, _665, _681, log_rw_709

6.3 Uncertainty NN

This NN is used to determine the uncertainties of the IOPs, which are the output of the inverse NN.

The data set for training of this NN has been computed using the training data set for the inverse NN and the corresponding output of the inverse NN. So for each case of this data set also the deviation is known. This can be used to train a NN with the 5 IOPs as input and the deviation (bias and scatter) as output, also for each of the 5 IOPs.

First the biasNN is trained and used to perform the bias correction of the training data set. In the next step the uncertainty NN is trained

The input of this NN are the log of the IOPs, the output are the absolute difference between the modeled IOPs and the output IOPs from the inverse IOP NN. Since this is the difference between the logs of the IOPs it is a measure of the relative uncertainty.

The absolute uncertainty (as presented in the validation chapter of this ATBD) is then calculated as $\exp(\log_a_iop_nn + \text{diff_log_abs_iop})$, where $\log_a_iop_nn$ is the output of the inverseNN (and input to the uncertainty NN) and diff_log_abs_iop is the output of the uncertainty NN.

the net has 5 inputs:

	DOC:	MERIS Case 2 water ATBD 4 th reproc		
	DATE:	20150319		
	Issue:	2	Revision:	
				Page: 20 of 55

input 1 is log_a_pig_nn
input 2 is log_a_det_nn
input 3 is log_a_gelb_nn
input 4 is log_b_spm_nn
input 5 is log_b_wit_nn

the net has 5 outputs:

output 1 is diff_log_abs_apig
output 2 is diff_log_abs_adet
output 3 is diff_log_abs_agelb
output 4 is diff_log_abs_bpart
output 5 is diff_log_abs_bwit

7 Optional NNs

7.1 Atmospheric transmittance

This NN determines the angular dependent downward and upward directed transmittance of the atmosphere in 12 MERIS bands.

Input variables are as for the *Rpath* and *Rw* NNs. Output are *td* and *tu*, both in 12 MERIS bands.

7.2 *kd_490*, *kd_min* and *z90_max*

The attenuation coefficient of the downwelling irradiance at 490 nm and the same at the MERIS band with minimum *kd* (*kd_min*) is computed. The $1/kd_min$ is then the signal depth *z90* (depth from which 90% of the radiance at the surface stems from) at the wavelength with maximum transparency. *z90_max* is related to the secchi disc depth.

7.3 Normalisation of *Rw*

This network normalises the directional *Rw*, which are output of the *Rw_invNN* (s. 5.1.2).

Normalisation is defined here the *Rw* for the sun in zenith and a nadir view, denoted here as *Rwn*.

Input is the same as the inverse IOP_NN (s. 6.1). Output are the corresponding 10 *Rwn*.

*Note: the input to the water NNs are always the directional *Rw* together with the sun and viewing angles.*

8 Computation of chlorophyll and total suspended matter, TSM

The concentrations of chlorophyll and total suspended matter dry weight are computed from the IOPs. The conversion factors have been determined by regression from water samples and corresponding IOP measurements mainly of the North Sea. Due to the simple and direct relationships, it is possible for the user to get the IOPs from the concentrations and apply their own conversion factors, which might be better adapted to their region of interest.

// compute concentrations

```
chl_a_nn1 =21.0.*(ap_a_nn1)^(1.04);
```

	DOC:	MERIS Case 2 water ATBD 4 th reproc		
	DATE:	20150319		
	Issue:	2	Revision:	Page: 21 of 55

`tsm_a_nn1 = btot_a_nn1*1.73;`

9 Computation of out-of-range, out-of-scope and uncertainties

9.1 Out-of-range flags

The tosa-out-of-range flag is triggered when any of the input variables of the atmosphere NNs is outside its minimum and maximum. The minima and maxima are included in the NNs.

The water-out-of-range flag is triggered when any of the input variables to the `rw_iop_NN` is outside its minimum and maximum.

The procedure to trigger the out-of-range flag is given here in *Scilab* notation for *Rtosa*:

```
// test if the input to the NN is out of range
// minima and maxima of aaNN input, also valid for all other AC NNs, retrieved from the NN itself
// mima: matrix of minima and maxima retrieved from the corresponding table of the NN
mima=aa_rtosa_nn_bn7_9(5);
tosa_oor_flag=0; // reset the flag
for iv=1:19, // test all NN input variables
    if nn_in(iv)< mima(iv,1)| nn_in(iv)> mima(iv,2)
        tosa_oor_flag(ipix)=1; // set flag if true
    end
end
end
```

9.2 Out-of-scope reflectances and flags

The out-of-scope procedures test if the absolute values and the shape of the input spectrum are within the scope of the training data set.

For the TOSA reflectances *Rtosa* the auto-associative neural network is used (s. chapter 5.1.1).

The out-of-scope degree and flag is set according to the following procedure, given in *Scilab* notation:

```
// test out of scope spectra with autoassociative neural network
log_rtosa_aann=nnhs_ff(aa_rtosa_nn_bn7_9,nn_in); // call of the NN
rtosa_aann=exp(log_rtosa_aann);
rtosa_aaNNrat= (rtosa_aann./r_tosa); // compute the ratio for all 12 bands
// set rho_toa out of scope flag
rtosa_aaNNrat_min=min(rtosa_aaNNrat); // compute minimum and maximum of all ratios
rtosa_aaNNrat_max=max(rtosa_aaNNrat);
// compute maximum ratio after inverting the minimum ratio, this value can be used to provide a
product of the out-of-scope degree.
rtosa_aaNNrat_minmax_a(ipix) = max([rtosa_aaNNrat_max(1.0./rtosa_aaNNrat_min)]);
```

	DOC:	MERIS Case 2 water ATBD 4 th reproc		
	DATE:	20150319		
	Issue:	2	Revision:	
				Page: 22 of 55

```
flag_rtosa(ipix)=0;
if rtosa_aaNNrat_min < thresh_rtosaaaNNrat(1) | rtosa_aaNNrat_max > thresh_rtosaaaNNrat(2) then
    flag_rtosa(ipix)=1; // set out-of-scope flag if ratios outside thresholds
end
```

For the water reflectance spectrum R_w this test is performed by combining the inverse and forward NN (s. chapters 6.1 and 6.2). That means the output of the inverse NN, which are the IOPs are used as input to the forward NN, the output of which is again a reflectance spectrum, R_w' .

To detect out of scope reflectance spectra two band reflectance ratios R_{w_560}/R_{w_412} and R_{w_620}/R_{w_560} are compared in the following way:

```
// compute the test and set rw is out of scope flag
s1_mess=abs(log_rw(5)-log_rw(2)); // s1_mess and s2_mess are the band ratios of Rw
s2_mess=abs(log_rw(6)-log_rw(5));
s1_nn2=abs(log_rw_nn2(5)-log_rw_nn2(2)); // s1_nn2 is the band ratios of Rw'
s2_nn2=abs(log_rw_nn2(6)-log_rw_nn2(5));
s1_test=exp(abs(s1_nn2-s1_mess)); // relative deviation for band ratio 5/2
s2_test=exp(abs(s2_nn2-s2_mess)); // relative deviation for band ratio 6/5
s12_test=max(s1_test,s2_test); // maximum deviation output as quality indicator
if s1_test > thresh_rwslope(1) | s2_test > thresh_rwslope(2) then
    flag_rw=1
else
    flag_rw=0;
end
```

The degree of the relative deviation, i.e. the maximum ratio, can be used as a quality parameter. If one of the two ratios surmount pre-defined thresholds, the out-of-scope flag is triggered.

9.3 Uncertainties of IOPs

The uncertainties of the retrieved IOPs are determined here as the difference between the retrieved IOPs and the corresponding modelled IOPs. For this purpose a uncertainty NN is trained (s. chapter 6.3 on page 19). It is based on a data set with the modelled IOPs, which have been used to train all water NNs, and the output of the inverse IOP NN. Since the final output products of the case 2 water procedure are *adg* and *TSM*, the uncertainties of these 2 combined variables have to be computed, which is less than the individual components *ad*, *ag*, *bp* and *bw*. In addition also the uncertainties of *kd490* and *kdmin* are computed with corresponding NNs.

The following procedure is used:

```
// NN compute uncertainties of individual IOPs
diff_log_abs_iop=nnhs_ff(unc_biasec_nn1,log_iops_nn1); // call of NN
// relative uncertainty
```

 BROCKMANN CONSULT	DOC:	MERIS Case 2 water ATBD 4 th reproc		
	DATE:	20150319		
	Issue:	2	Revision:	

```

unc_iop_rel(ipix,:)=(exp(diff_log_abs_iop)-1).*100;
// absolute uncertainty
unc_iop_abs(ipix,:)=iop_nn1(ipix,:).*(1.0-exp(-diff_log_abs_iop));

// compute uncertainty of chlorophyll from uncertainty of apig == unc_iop_abs(ipix,1)
unc_abs_chl(ipix) = 21.0.*unc_iop_abs(ipix,1).^(1.04);

// NN compute uncertainties for combined IOPs and kd
diff_log_abs_combi_kd=nnhs_ff(unc_biase_atotkd_nn,log_iops_nn1); // call of NN
diff_log_abs_adg = diff_log_abs_combi_kd(1);
diff_log_abs_atot = diff_log_abs_combi_kd(2);
diff_log_abs_btot = diff_log_abs_combi_kd(3);
diff_log_abs_kd489= diff_log_abs_combi_kd(4);
diff_log_abs_kdmin= diff_log_abs_combi_kd(5);

unc_abs_adg = (1.0-exp(-diff_log_abs_adg)).* adg_a_nn1;
unc_abs_atot = (1.0-exp(-diff_log_abs_atot)).* atot_a_nn1;
unc_abs_btot = (1.0-exp(-diff_log_abs_btot)).* btot_a_nn1;
unc_abs_kd489 = (1.0-exp(-diff_log_abs_kd489)).*kd489_nn;
unc_abs_kdmin = (1.0-exp(-diff_log_abs_kdmin)).*kdmin_nn;
// compute uncertainty of TSM from btot, 1.73 is the conversion factor btot-> TSM
unc_abs_tsm = 1.73.*unc_abs_btot;

```

	DOC:	MERIS Case 2 water ATBD 4 th reproc		
	DATE:	20150319		
	Issue:	2	Revision:	
				Page: 24 of 55

10 Validation of the algorithms

The performance of the procedure with the NNs as described above has been tested with two different data sets: (1) a set of transects in the North Sea (German Bight) from the estuary of the river Elbe to the island of Helgoland. This transect covers different water types from very turbid to clear sea water. (2) The other data set is MERMAID, which has been compiled by ACRI for ESA for the validation of MERIS data, mainly for testing the calibration of MERIS together with the atmospheric correction. It covers mainly clear oceanic water types. It consists of various sources from different contributors worldwide including data of optical buoy MOBY (Hawaii), BOUSSOLE (Mediterranean Sea off Villefranche sur Mer), AAOT (Venice Tower) and various stations of the Ocean Colour AERONET.

10.1 Validation using data of the Helgoland transects

This data set consists of 9 transects of in situ samples, which were taken between Cuxhaven and the island of Helgoland in the North Sea / German Bight. One of these transects (C18) was located between the harbour of Büsum and Helgoland. Along the transects the water changes from turbid estuarine water to blue-green water with a secchi disc depth of > 6 m. This transects offer a large variety of the concentration of all optically relevant water constituents. However, one has to consider that the coastal water is very patchy with strong tidal currents so that differences have to be expected between the results taken from MERIS pixels and the water samples.

Measurements were performed from the Ferry boat, which runs every day during summer months.

The reflectance of the water was measured continuously during the cruise with a TRIOS Ramses Spectrometer system from the bow of the ship, where the water is undisturbed during cruising. This system consists of 3 spectrometers, one is pointing to the water surface under a nadir angle of 45 degrees, the second one is pointing to the sky under the corresponding angle to determine the reflected sky light and the third spectrometer is used to measure the downwelling irradiance. Azimuth angle with respect to the sun was about 135 degrees. Water samples were taken during the cruise from the water surface and processed for phytoplankton pigments, suspended matter and the absorption by particulate matter and the filtered water.

In the following sections the results of the comparison will be presented and discussed for all 9 transects in temporal order.

10.1.1 Transect C18 20050420

This is the only transect between the coastal town of Büsum and Helgoland. The coastal part crosses part of the shallow Waddensea, which is characterized by very turbid water and narrow channels and partly dry fallen sand and mud flats.

	DOC:	MERIS Case 2 water ATBD 4 th reproc		
	DATE:	20150319		
	Issue:	2	Revision:	Page: 25 of 55

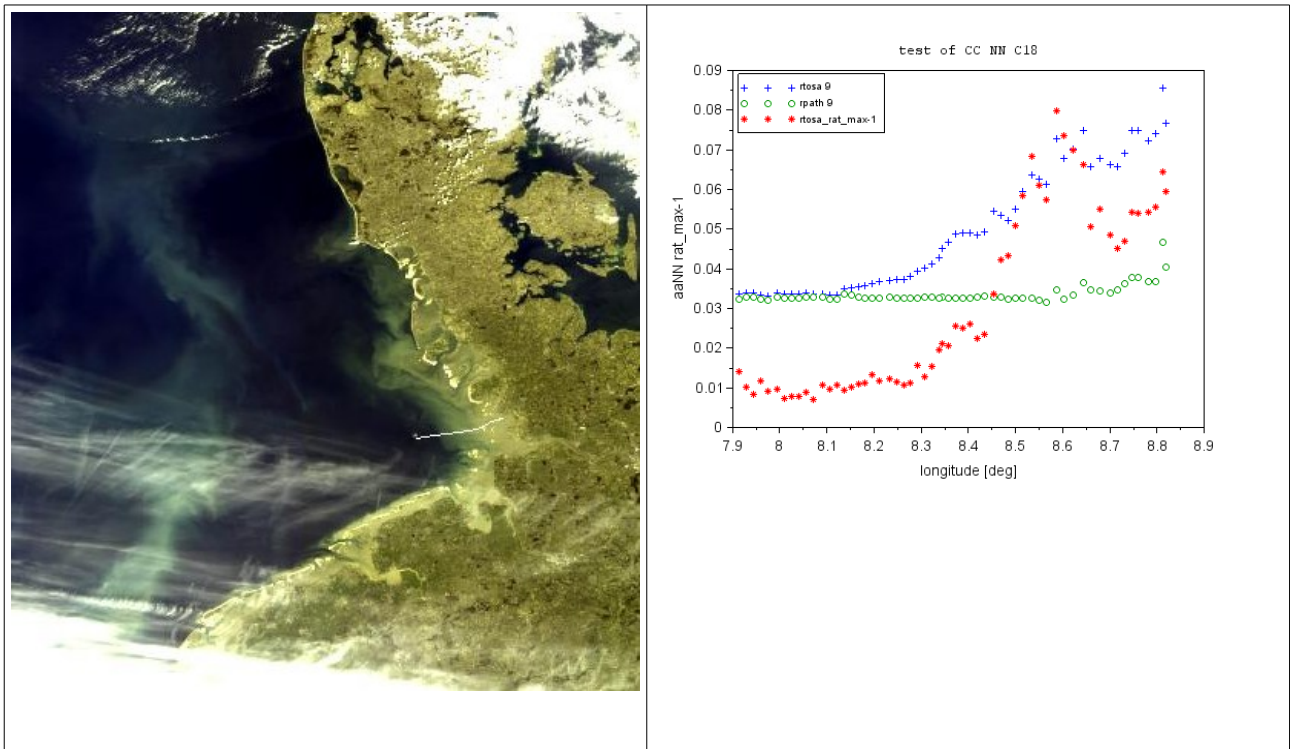


Fig. 14: Transect C18 (20.4.2014) between Büsum and Helgoland with the track in the MERIS L1b scene of this day (left) and the reflectance along this track of R_{tosa} (blue) and the path radiance R_{path} (green).

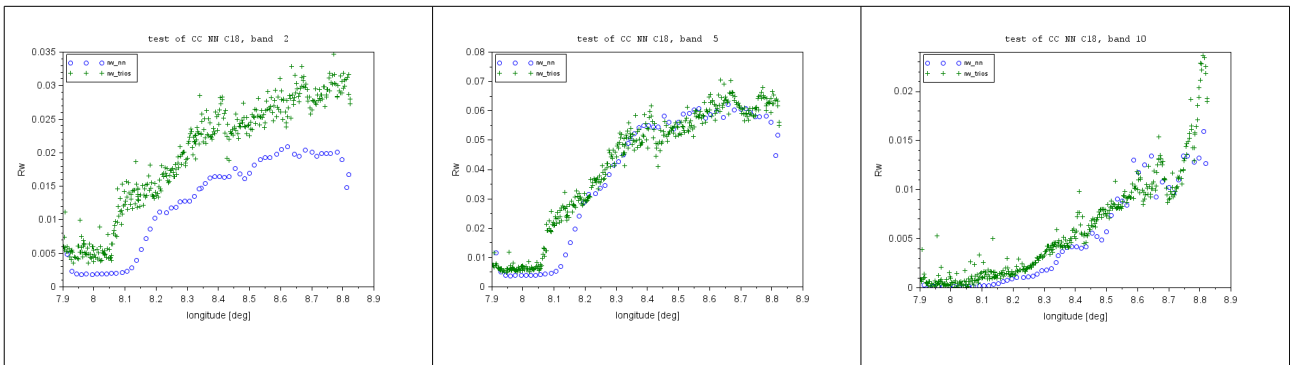


Fig. 15: Comparison of water leaving reflectances from MERIS and the TRIOS system.

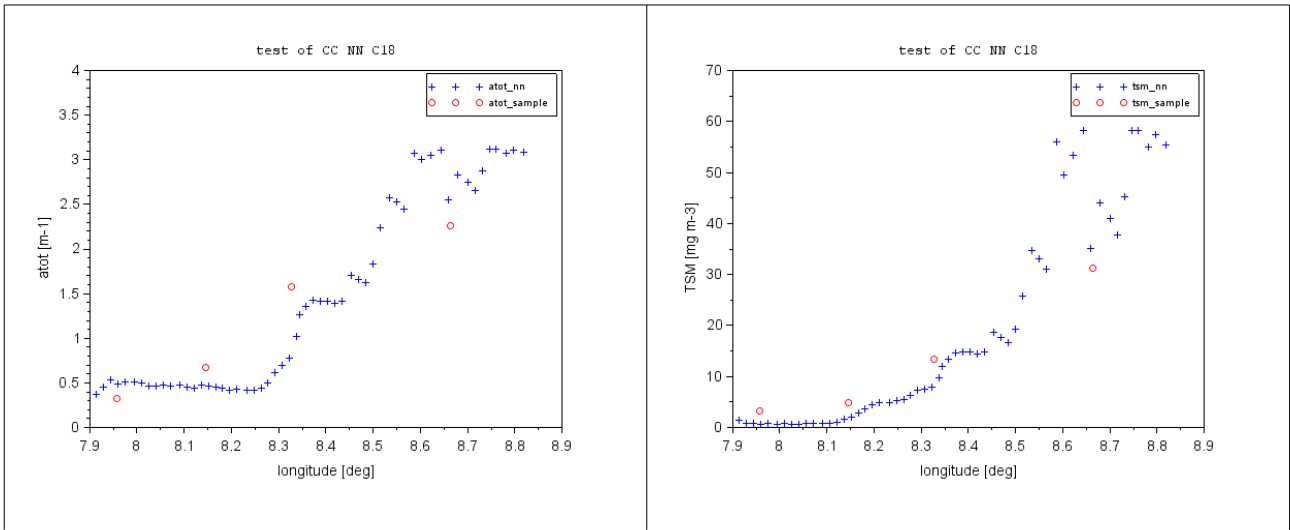


Fig. 16: Comparison between water samples (red) and MERIS data (blue) for the absorption coefficient(left) and total suspended matter dry weight (TSM) (right) of all water constituents.

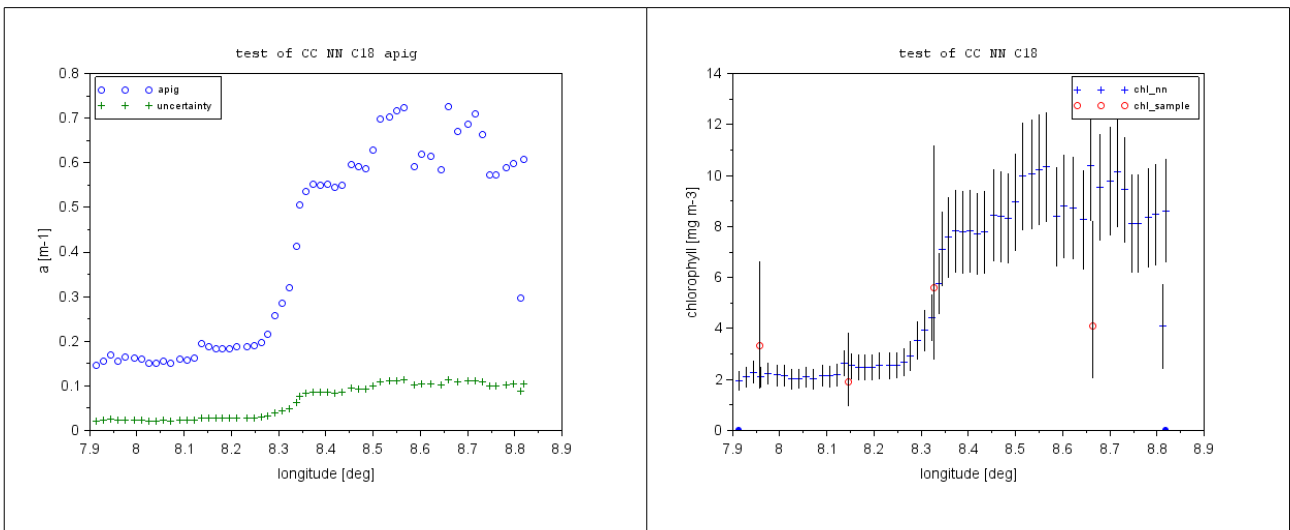


Fig. 17: Pigment absorption coefficient (left, blue) together with the uncertainty (green). On the right the corresponding chlorophyll concentration along the transect with the uncertainty range (vertical bars) and the chlorophyll concentration of the samples (red) with the factor 2 uncertainty range.

	DOC:	MERIS Case 2 water ATBD 4 th reproc		
	DATE:	20150319		
	Issue:	2	Revision:	Page: 27 of 55

10.1.2 Transect C23, 20050901

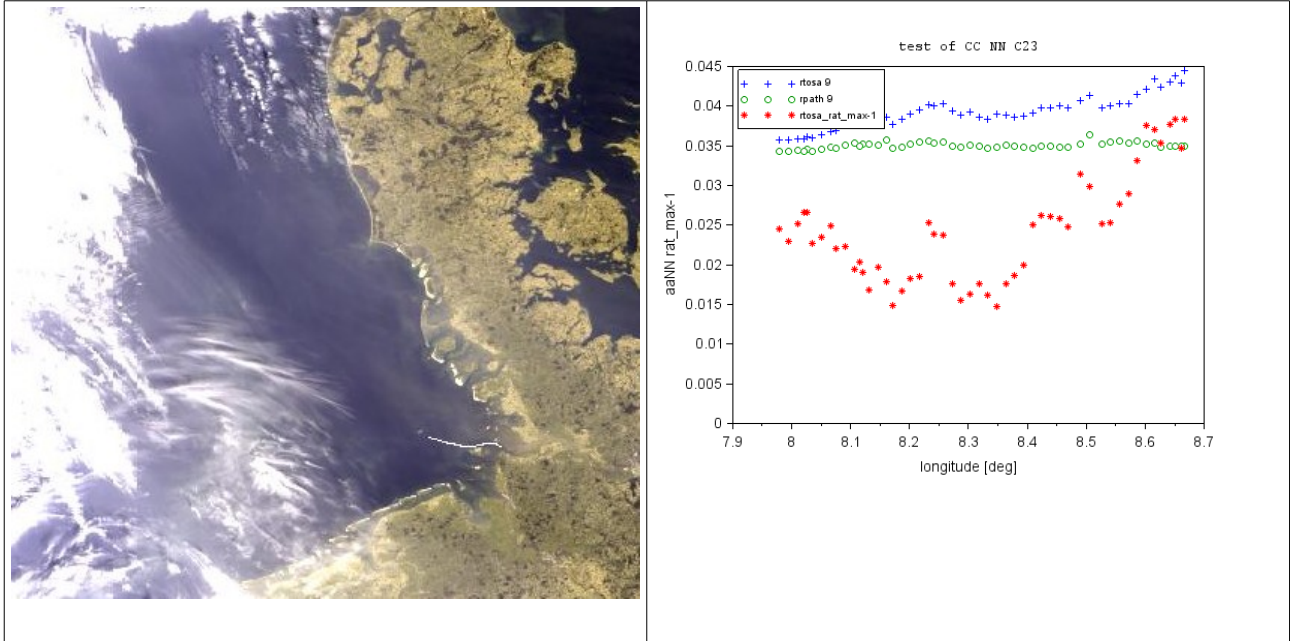


Fig. 18: Transect C23 (1.9.2005) between Cuxhaven and Helgoland with the track in the MERIS L1b scene of this day (left) and the reflectance along this track of Rtosa (blue) and the path radiance Rpath (green).

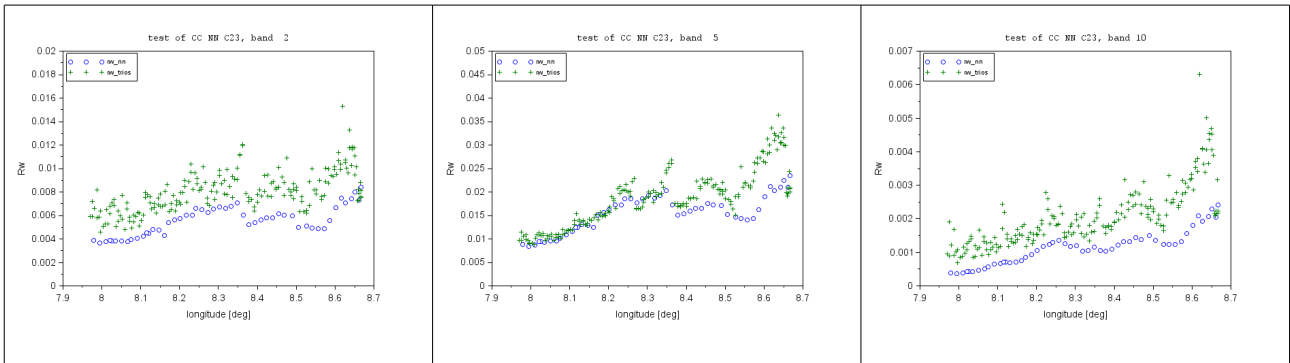


Fig. 19: Comparison of water leaving reflectances from MERIS and the TRIOS system.

	DOC:	MERIS Case 2 water ATBD 4 th reproc		
	DATE:	20150319		
	Issue:	2	Revision:	Page: 28 of 55

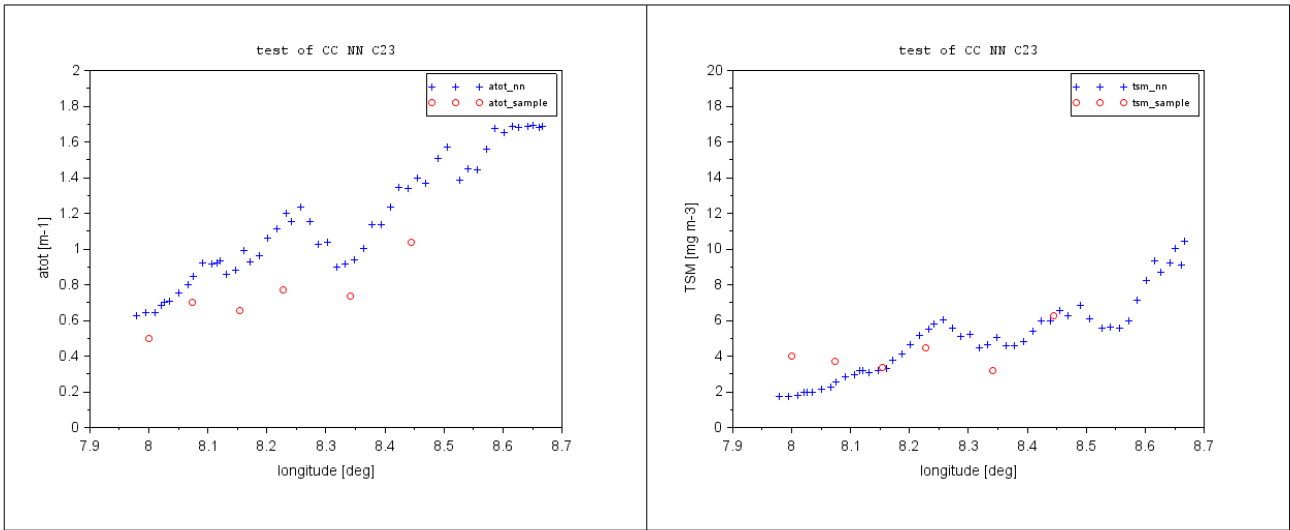


Fig. 20: Comparison between water samples (red) and MERIS data (blue) for the absorption coefficient (left) and total suspended matter dry weight (TSM) (right) of all water constituents.

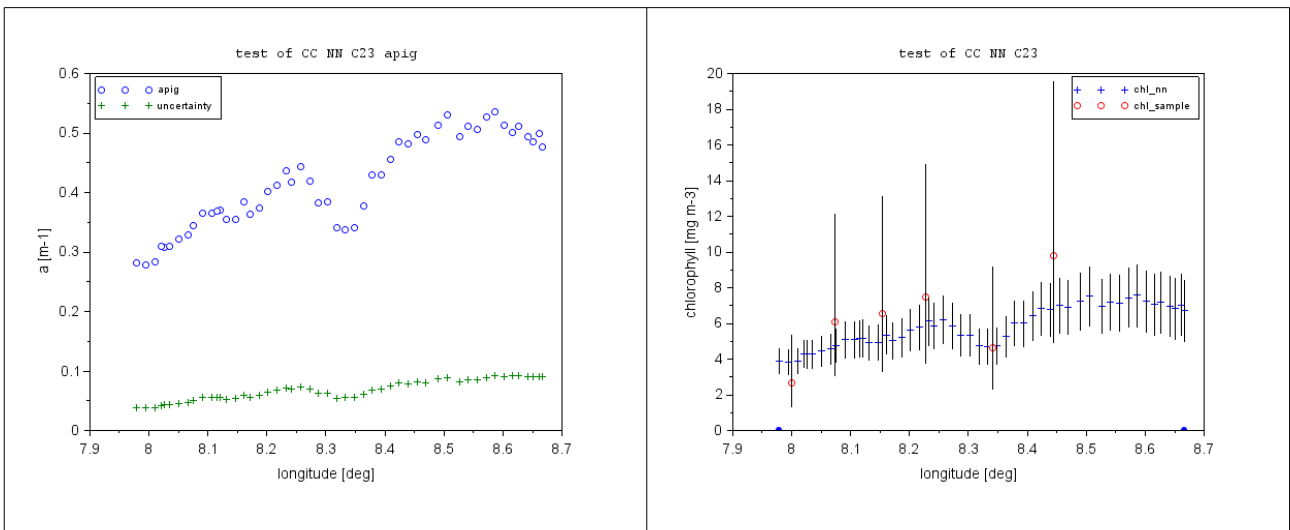


Fig. 21: Pigment absorption coefficient (left, blue) together with the uncertainty (green). On the right the corresponding chlorophyll concentration along the transect with the uncertainty range (vertical bars) and the chlorophyll concentration of the samples (red) with the factor 2 uncertainty range.

	DOC:	MERIS Case 2 water ATBD 4 th reproc		
	DATE:	20150319		
	Issue:	2	Revision:	Page: 29 of 55

10.1.3 Transect C24 20051006

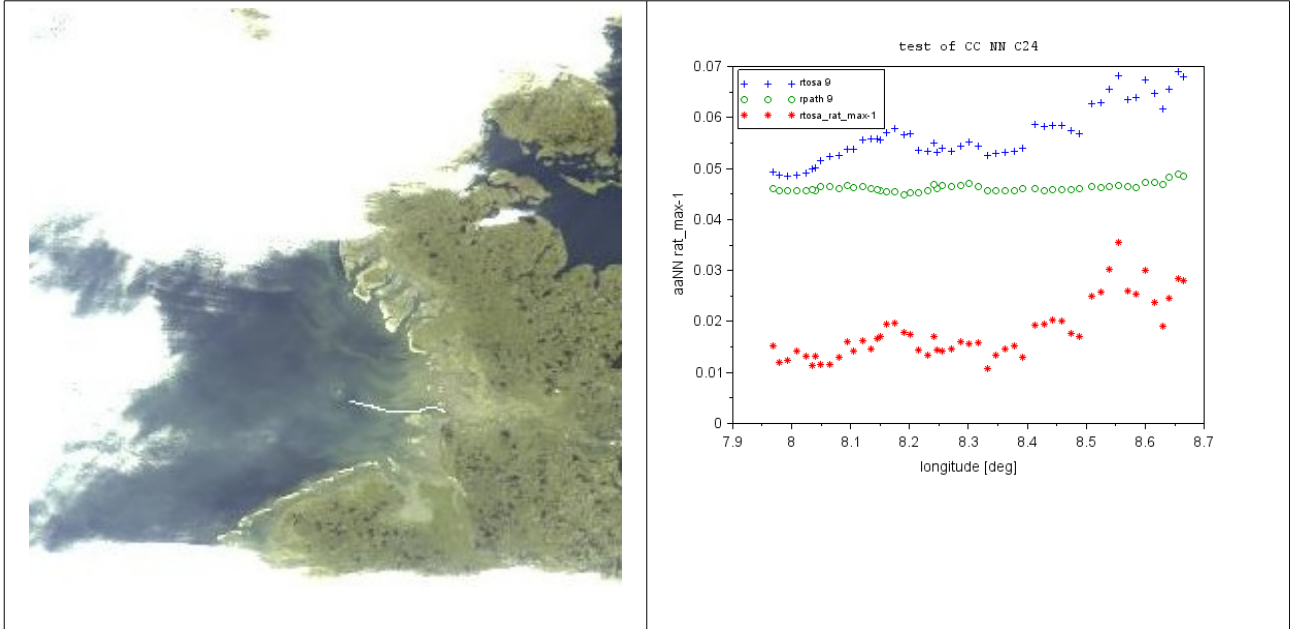


Fig. 22: Transect C24 (6.10.2005) between Cuxhaven and Helgoland with the track in the MERIS L1b scene of this day (left) and the reflectance along this track of Rtosa (blue) and the path radiance Rpath (green).

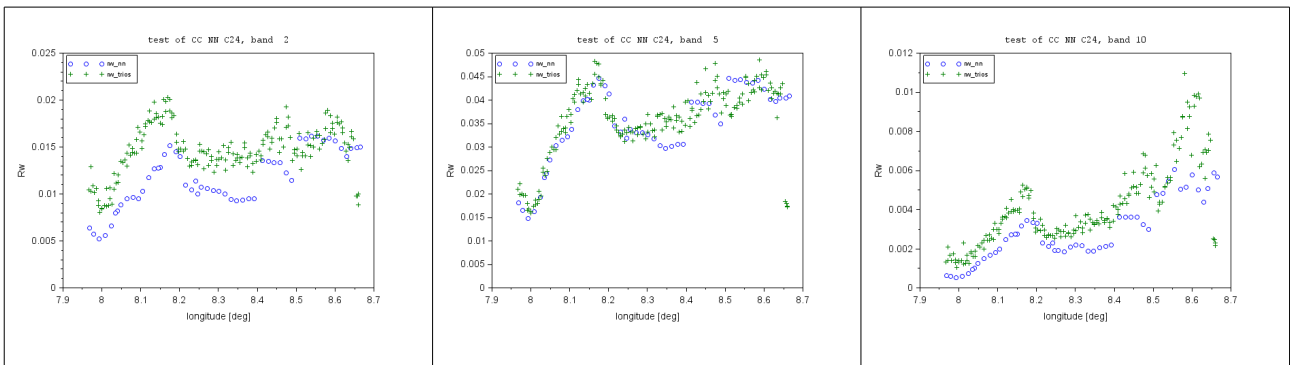


Fig. 23: Comparison of water leaving reflectances from MERIS and the TRIOS system.

	DOC:	MERIS Case 2 water ATBD 4 th reproc		
	DATE:	20150319		
	Issue:	2	Revision:	Page: 30 of 55

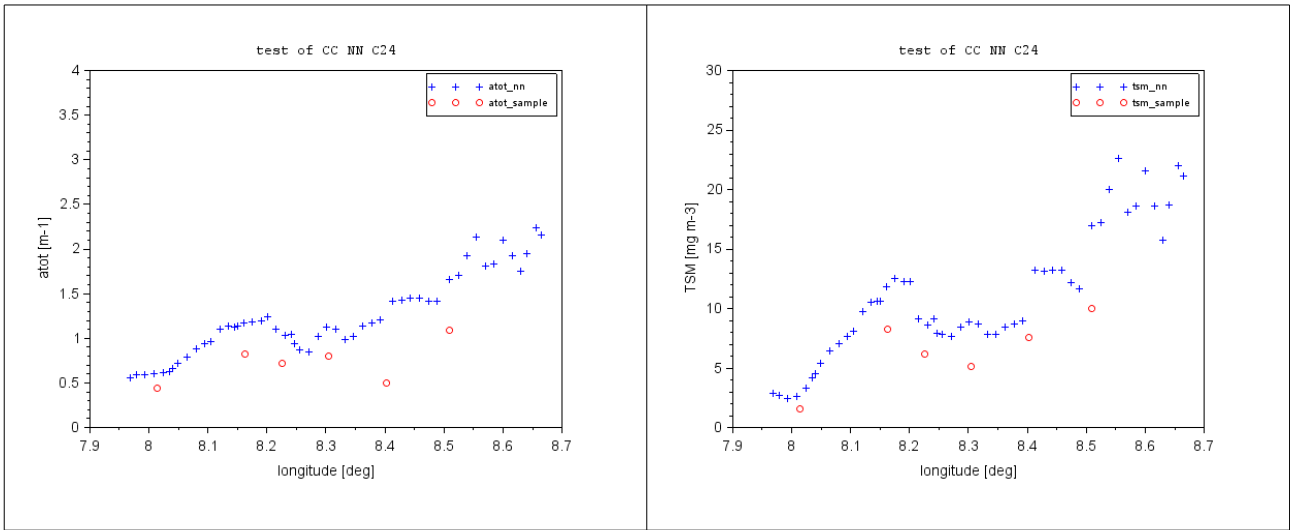


Fig. 24: Comparison between water samples (red) and MERIS data (blue) for the absorption coefficient(left) and total suspended matter dry weight (TSM) (right) of all water constituents.

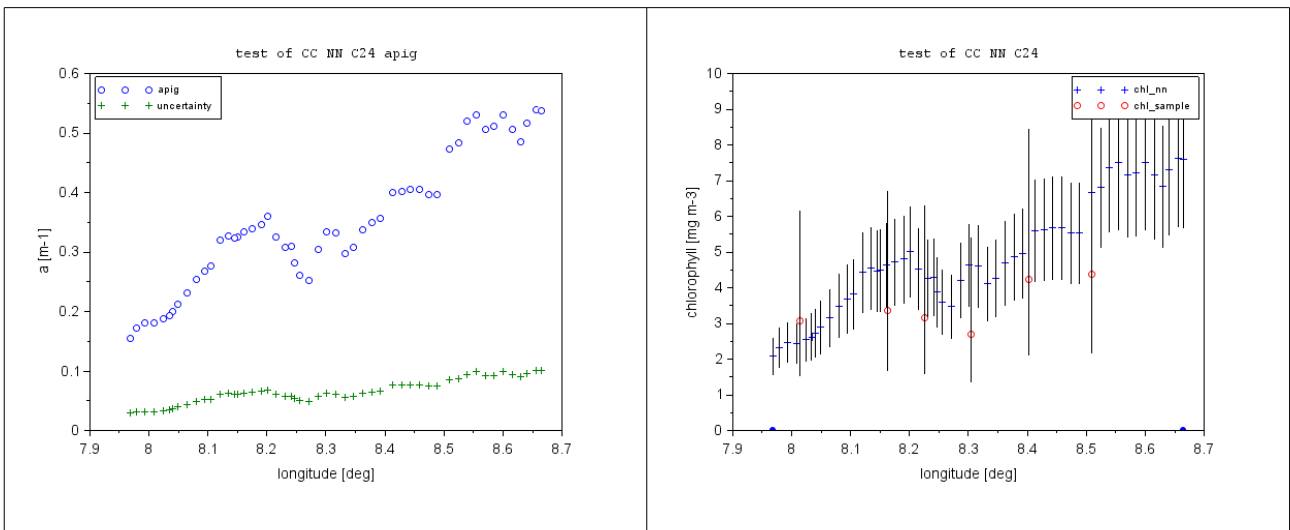


Fig. 25: Pigment absorption coefficient (left, blue) together with the uncertainty (green). On the right the corresponding chlorophyll concentration along the transect with the uncertainty range (vertical bars) and the chlorophyll concentration of the samples (red) with the factor 2 uncertainty range.

	DOC:	MERIS Case 2 water ATBD 4 th reproc		
	DATE:	20150319		
	Issue:	2	Revision:	Page: 31 of 55

10.1.4 Transect C25, 20051013

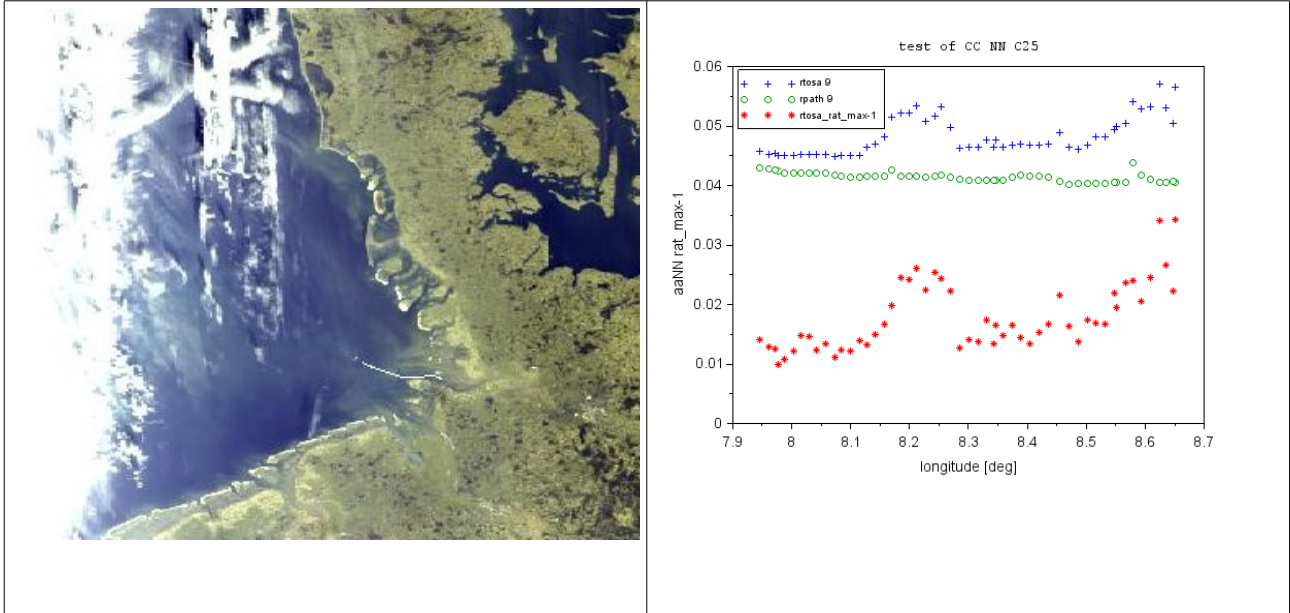


Fig. 26: Transect C25 (13.10.2005) between Cuxhaven and Helgoland with the track in the MERIS L1b scene of this day (left) and the reflectance along this track of Rtosa (blue) and the path radiance Rpath (green).

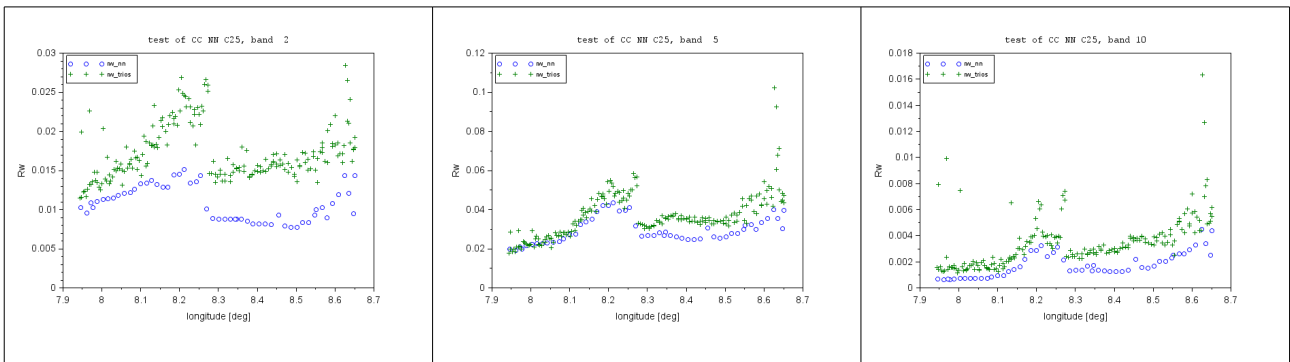


Fig. 27: Comparison of water leaving reflectances from MERIS and the TRIOS system.

	DOC:	MERIS Case 2 water ATBD 4 th reproc		
	DATE:	20150319		
	Issue:	2	Revision:	Page: 32 of 55

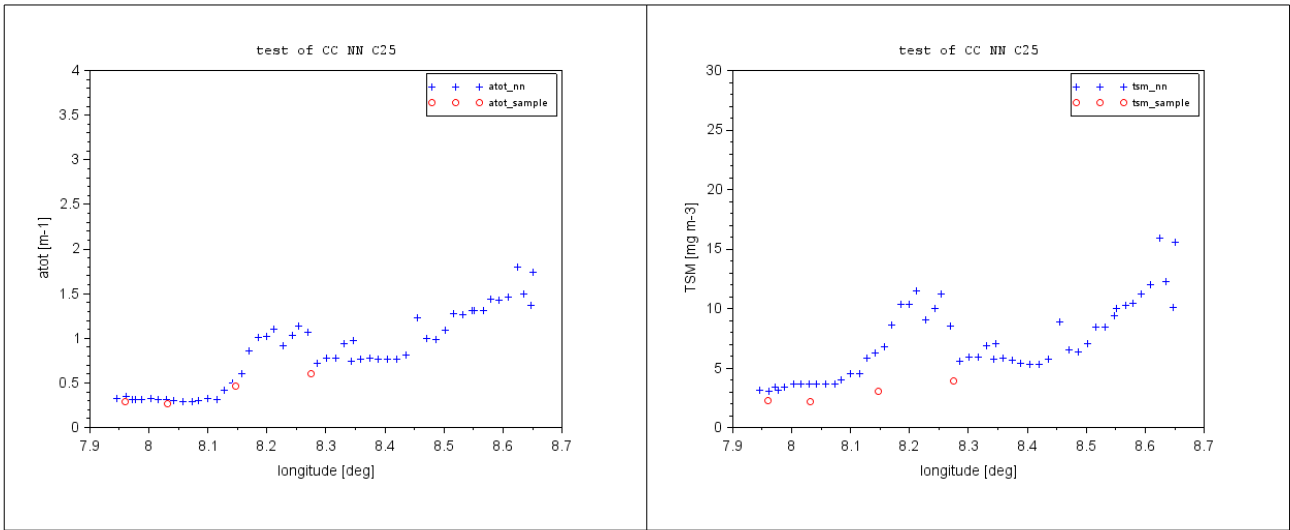


Fig. 28: Comparison between water samples (red) and MERIS data (blue) for the absorption coefficient(left) and total suspended matter dry weight (TSM) (right) of all water constituents.

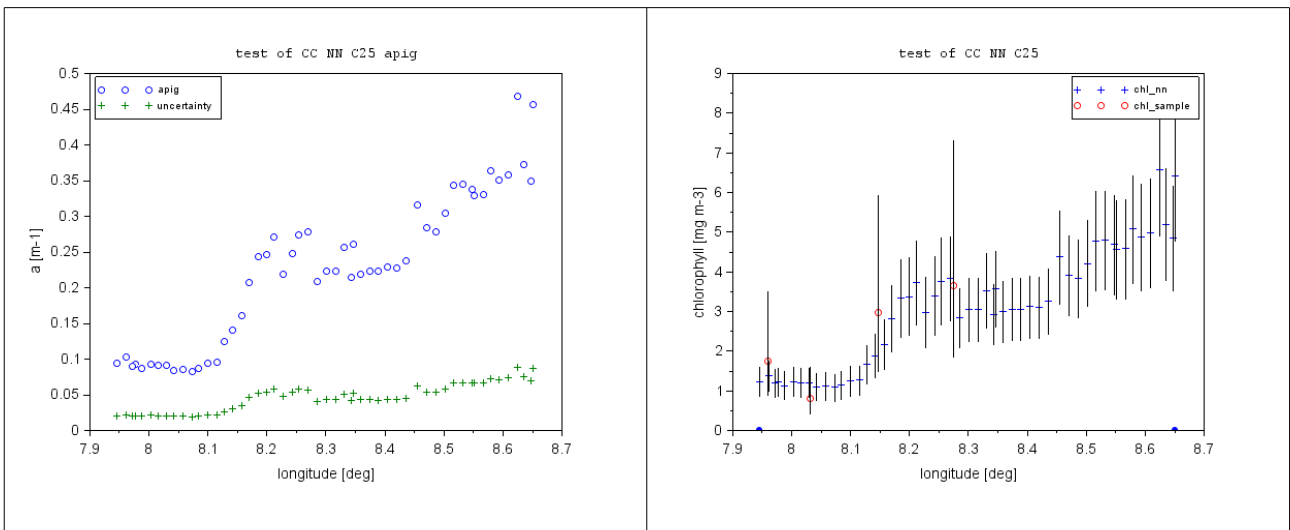


Fig. 29: Pigment absorption coefficient (left, blue) together with the uncertainty (green). On the right the corresponding chlorophyll concentration along the transect with the uncertainty range (vertical bars) and the chlorophyll concentration of the samples (red) with the factor 2 uncertainty range.

	DOC:	MERIS Case 2 water ATBD 4 th reproc		
	DATE:	20150319		
	Issue:	2	Revision:	Page: 33 of 55

10.1.5 Transect C26, 20060508

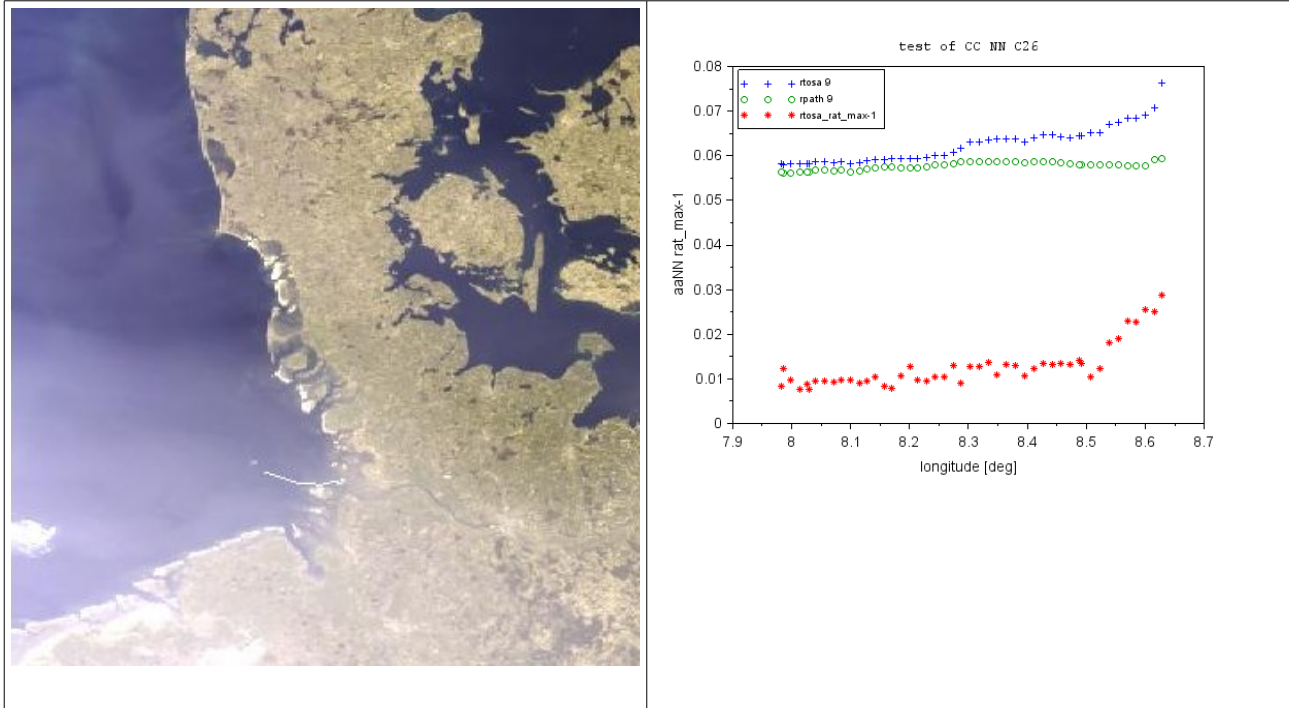


Fig. 30: Transect C26 (8.5.2006) between Cuxhaven and Helgoland with the track in the MERIS L1b scene of this day (left) and the reflectance along this track of Rtosa (blue) and the path radiance Rpath (green).

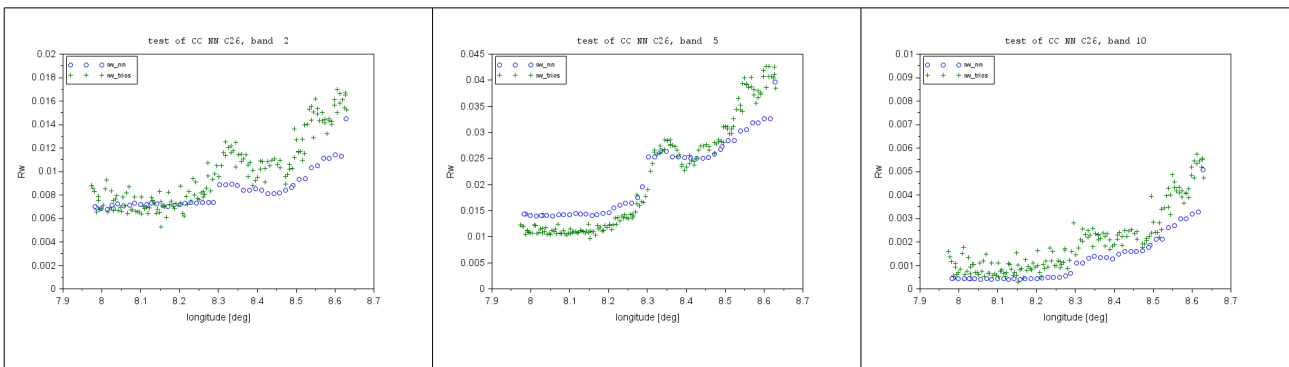


Fig. 31: Comparison of water leaving reflectances from MERIS and the TRIOS system.

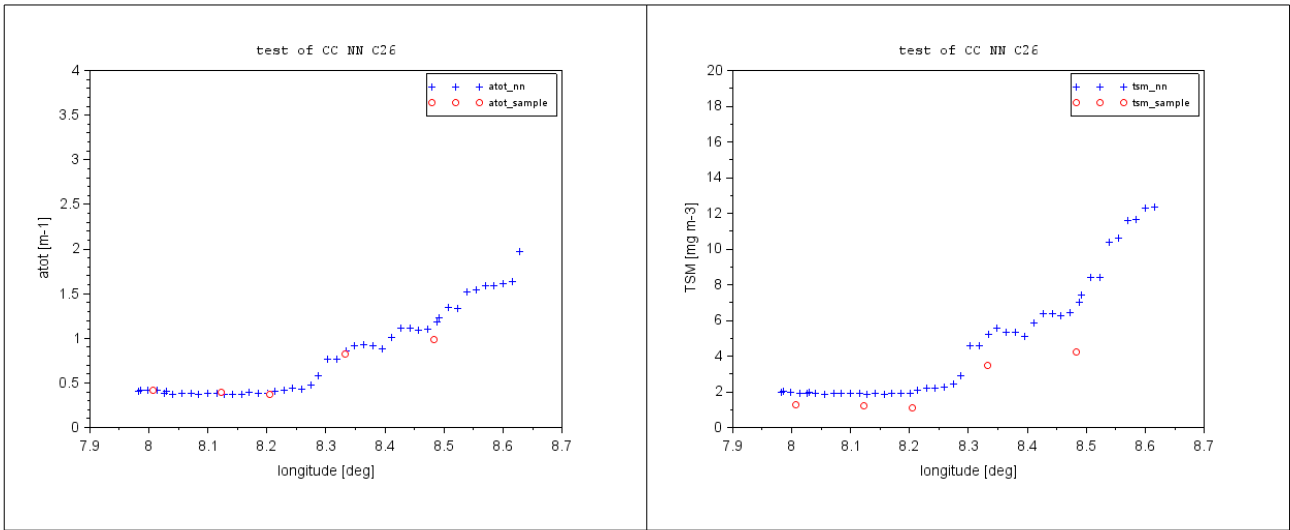


Fig. 32: Comparison between water samples (red) and MERIS data (blue) for the absorption coefficient (left) and total suspended matter dry weight (TSM) (right) of all water constituents.

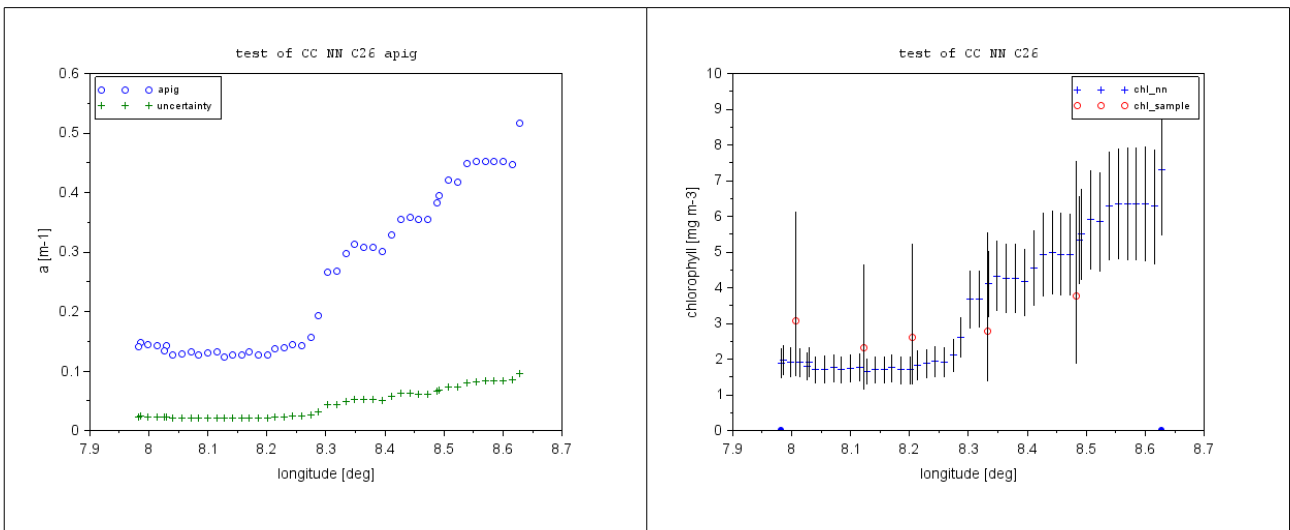


Fig. 33: Pigment absorption coefficient (left, blue) together with the uncertainty (green). On the right the corresponding chlorophyll concentration along the transect with the uncertainty range (vertical bars) and the chlorophyll concentration of the samples (red) with the factor 2 uncertainty range.

	DOC:	MERIS Case 2 water ATBD 4 th reproc		
	DATE:	20150319		
	Issue:	2	Revision:	Page: 35 of 55

10.1.6 Transect C27, 20060511

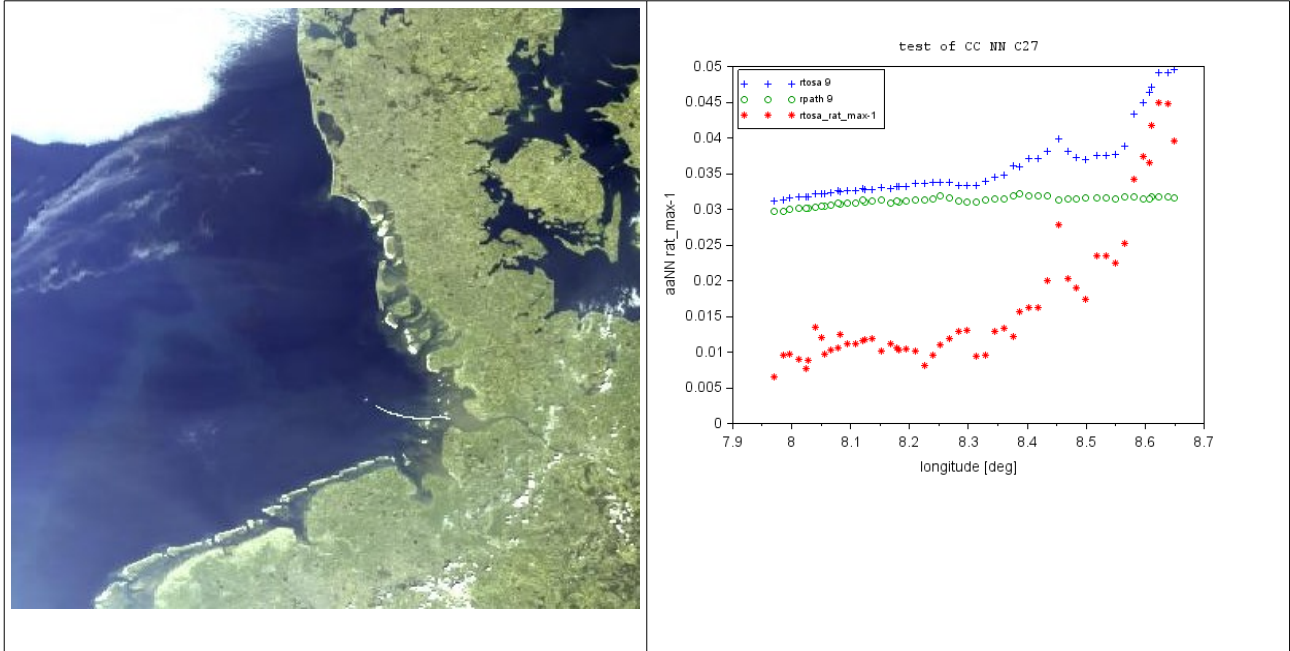


Fig. 34: Transect C27 (11.5.2006) between Cuxhaven and Helgoland with the track in the MERIS L1b scene of this day (left) and the reflectance along this track of Rtosa (blue) and the path radiance Rpath (green).

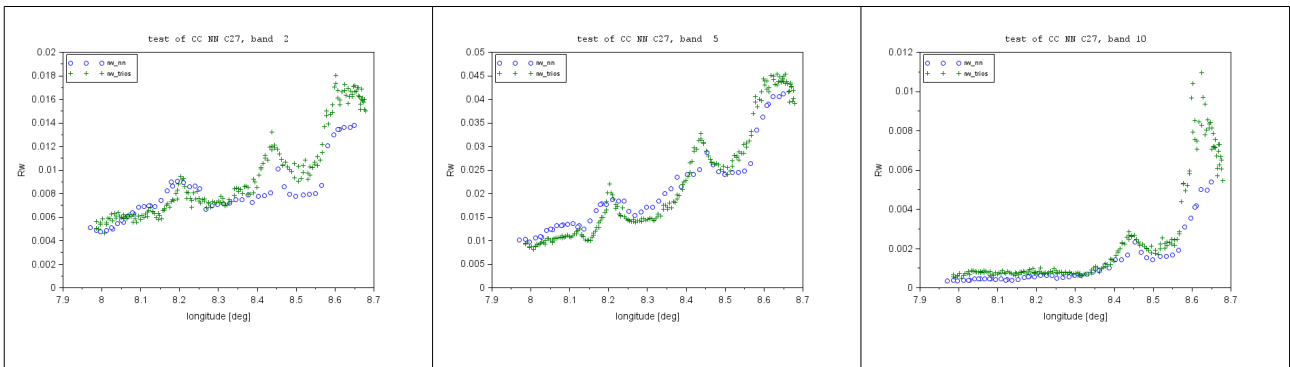


Fig. 35: Comparison of water leaving reflectances from MERIS and the TRIOS system.

	DOC:	MERIS Case 2 water ATBD 4 th reproc		
	DATE:	20150319		
	Issue:	2	Revision:	Page: 36 of 55

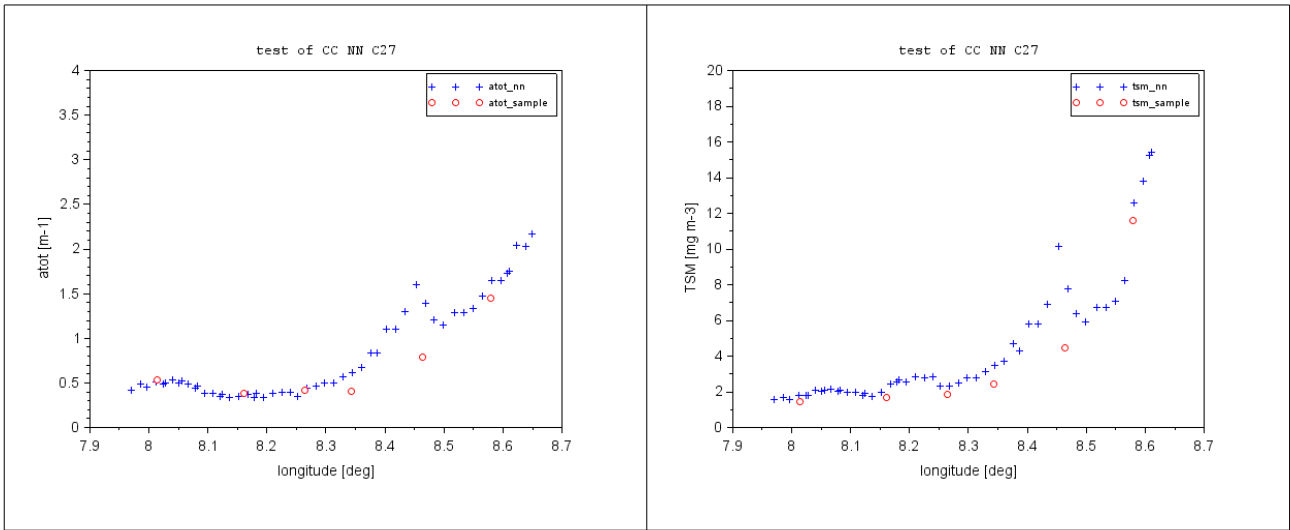


Fig. 36: Comparison between water samples (red) and MERIS data (blue) for the absorption coefficient (left) and total suspended matter dry weight (TSM) (right) of all water constituents.

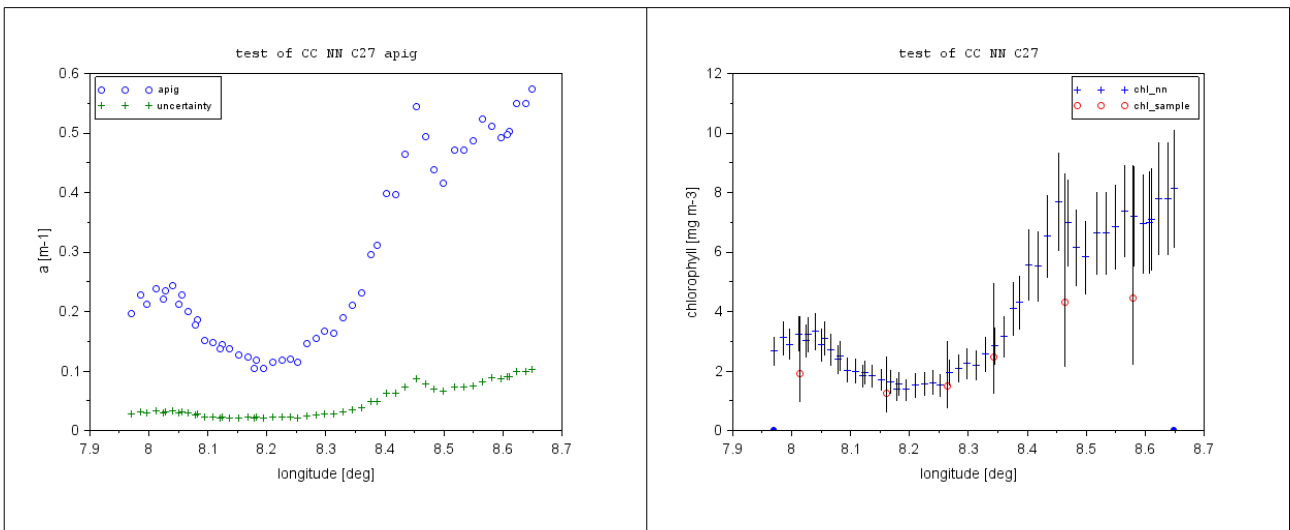


Fig. 37: Pigment absorption coefficient (left, blue) together with the uncertainty (green). On the right the corresponding chlorophyll concentration along the transect with the uncertainty range (vertical bars) and the chlorophyll concentration of the samples (red) with the factor 2 uncertainty range.

	DOC:	MERIS Case 2 water ATBD 4 th reproc		
	DATE:	20150319		
	Issue:	2	Revision:	Page: 37 of 55

10.1.7 Transect C28, 20060612

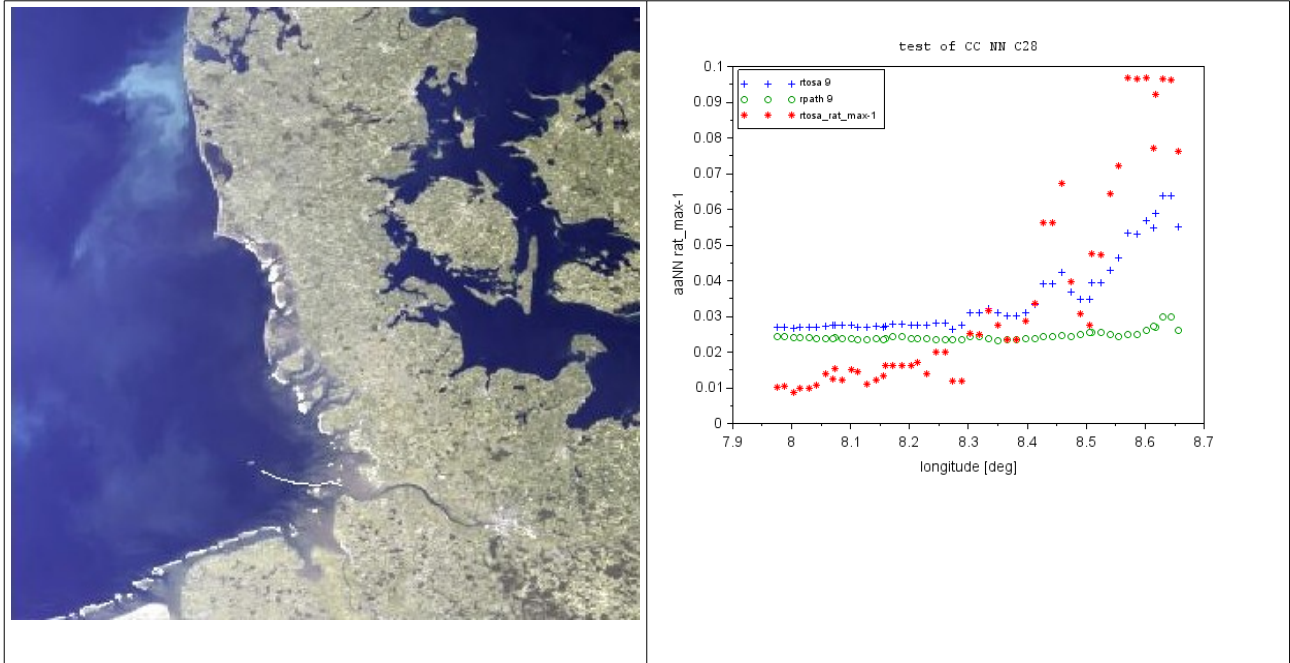


Fig. 38: Transect C28 (12.6.2006) between Cuxhaven and Helgoland with the track in the MERIS L1b scene of this day (left) and the reflectance along this track of R_{tosa} (blue) and the path radiance R_{path} (green).

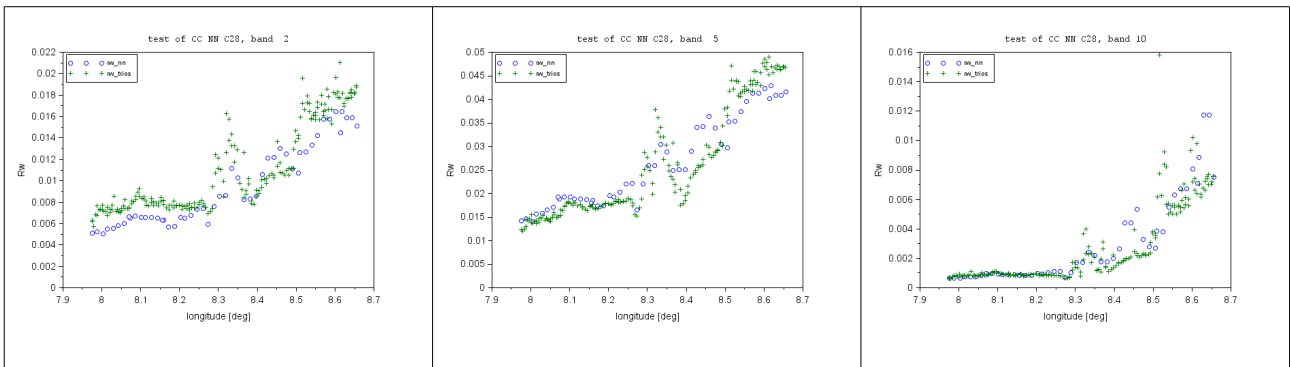


Fig. 39: Comparison of water leaving reflectances from MERIS and the TRIOS system.

	DOC:	MERIS Case 2 water ATBD 4 th reproc		
	DATE:	20150319		
	Issue:	2	Revision:	Page: 38 of 55

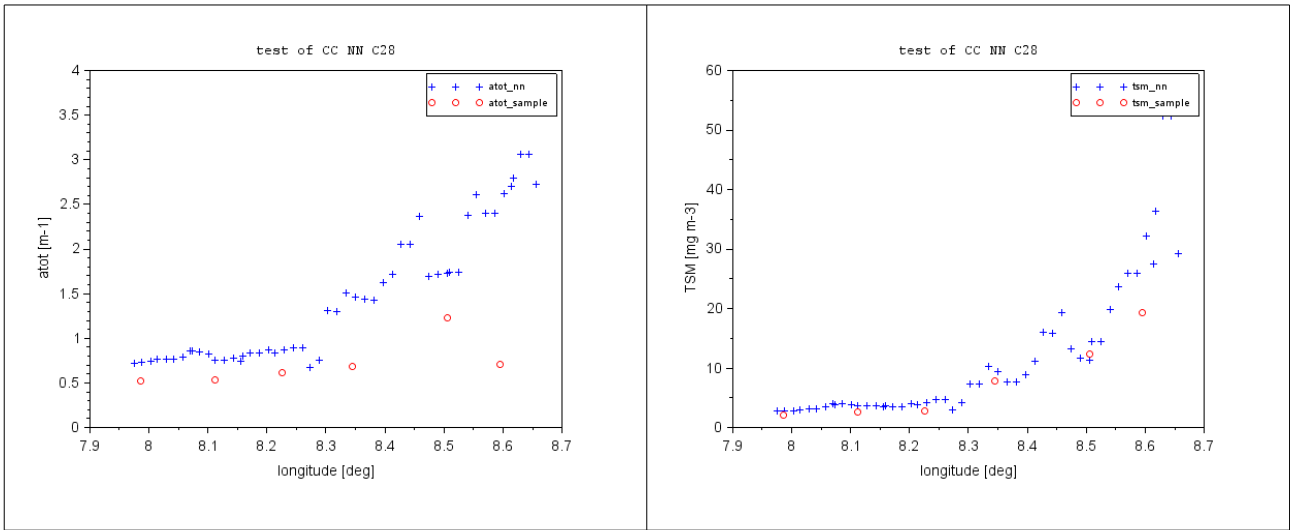


Fig. 40: Comparison between water samples (red) and MERIS data (blue) for the absorption coefficient (left) and total suspended matter dry weight (TSM) (right) of all water constituents.

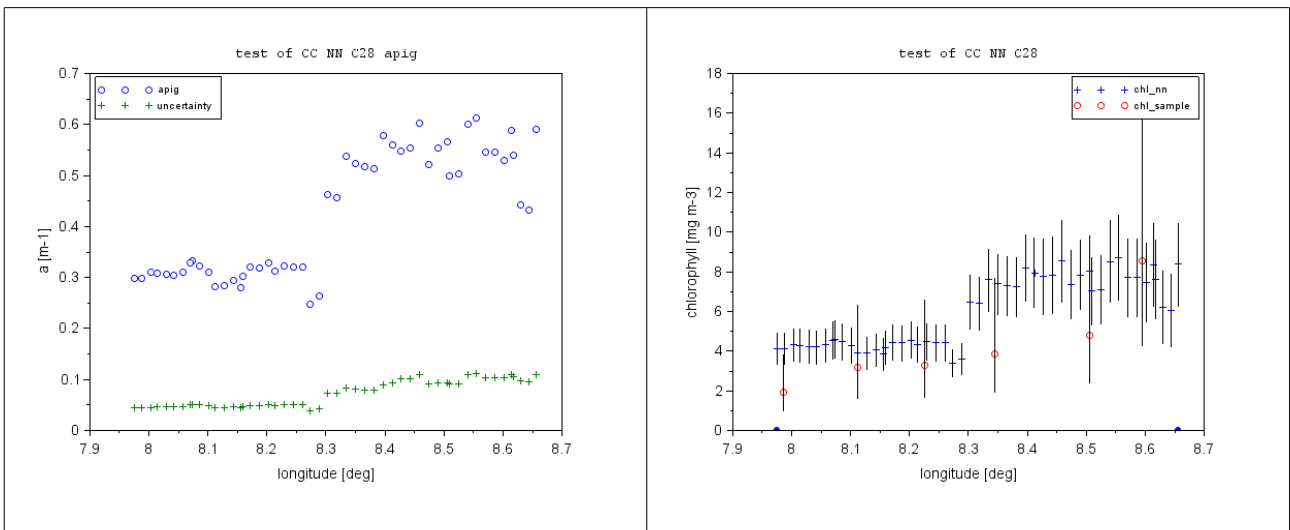


Fig. 41: Pigment absorption coefficient (left, blue) together with the uncertainty (green). On the right the corresponding chlorophyll concentration along the transect with the uncertainty range (vertical bars) and the chlorophyll concentration of the samples (red) with the factor 2 uncertainty range.

	DOC:	MERIS Case 2 water ATBD 4 th reproc		
	DATE:	20150319		
	Issue:	2	Revision:	Page: 39 of 55

10.1.8 Transect C29, 20060704

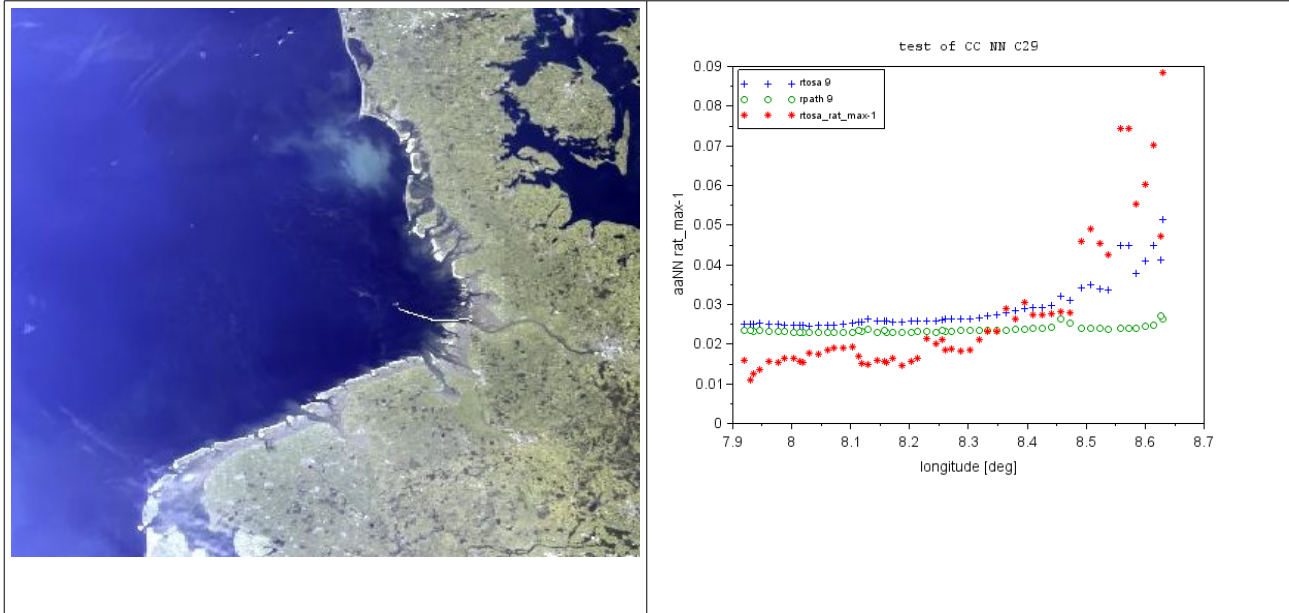


Fig. 42: Transect C29 (4.7.2006) between Cuxhaven and Helgoland with the track in the MERIS L1b scene of this day (left) and the reflectance along this track of Rtosa (blue) and the path radiance Rpath (green).

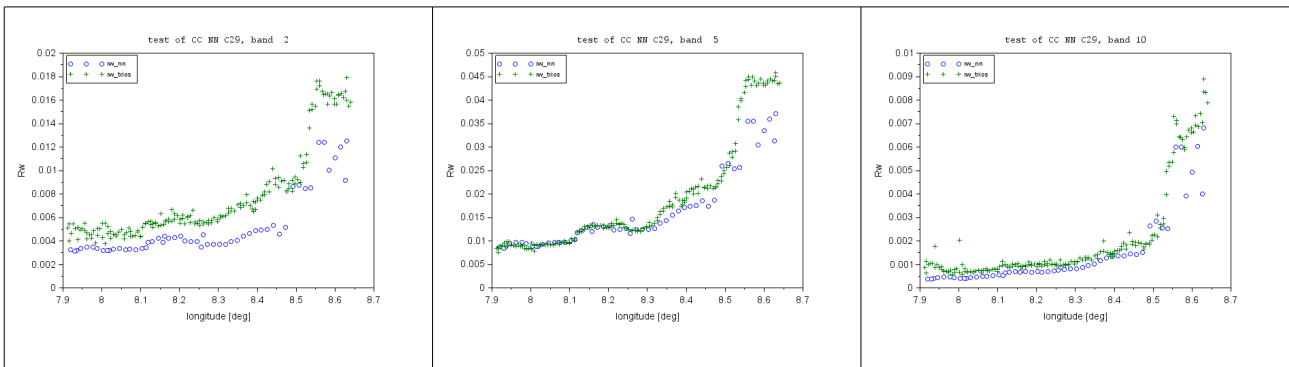


Fig. 43: Comparison of water leaving reflectances from MERIS and the TRIOS system.

	DOC:	MERIS Case 2 water ATBD 4 th reproc		
	DATE:	20150319		
	Issue:	2	Revision:	Page: 40 of 55

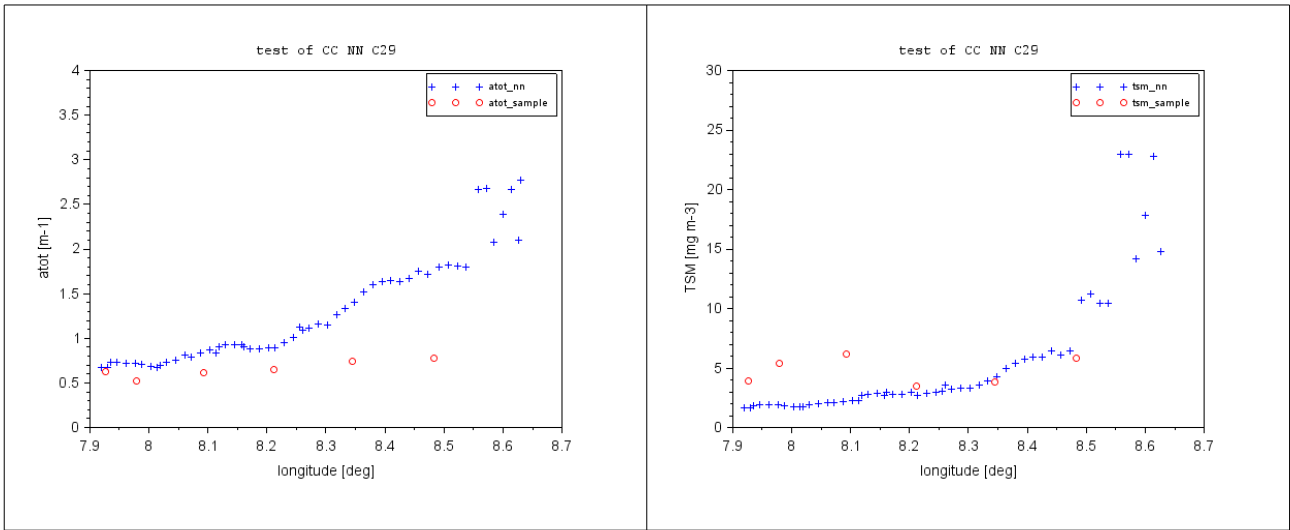


Fig. 44: Comparison between water samples (red) and MERIS data (blue) for the absorption coefficient(left) and total suspended matter dry weight (TSM) (right) of all water constituents.

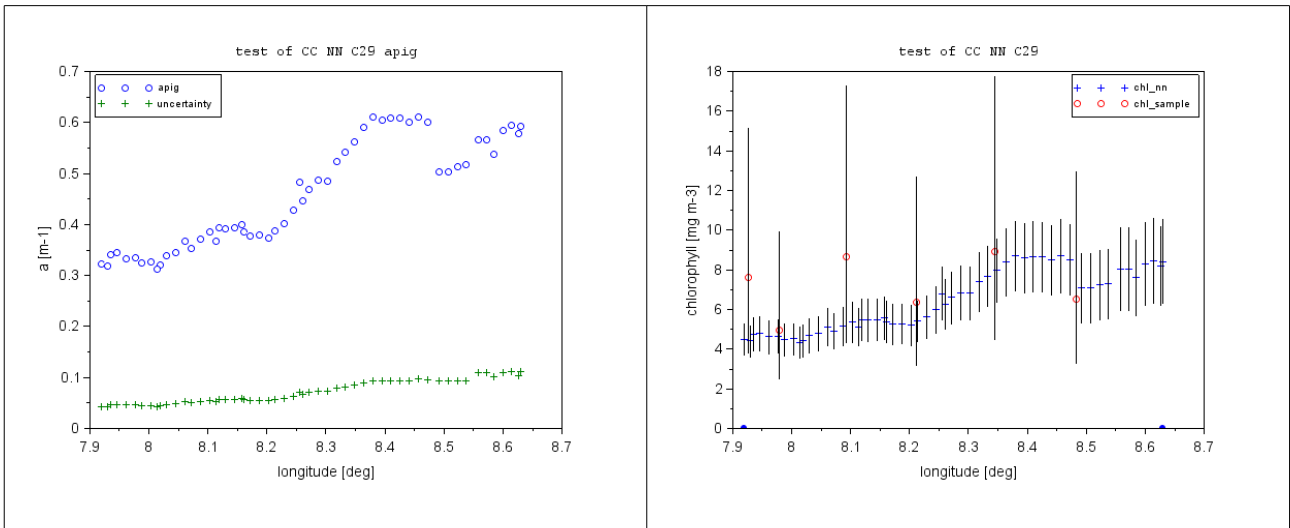


Fig. 45: Pigment absorption coefficient (left, blue) together with the uncertainty (green). On the right the corresponding chlorophyll concentration along the transect with the uncertainty range (vertical bars) and the chlorophyll concentration of the samples (red) with the factor 2 uncertainty range.

	DOC:	MERIS Case 2 water ATBD 4 th reproc		
	DATE:	20150319		
	Issue:	2	Revision:	Page: 41 of 55

10.1.9 Transect C32, 20060726

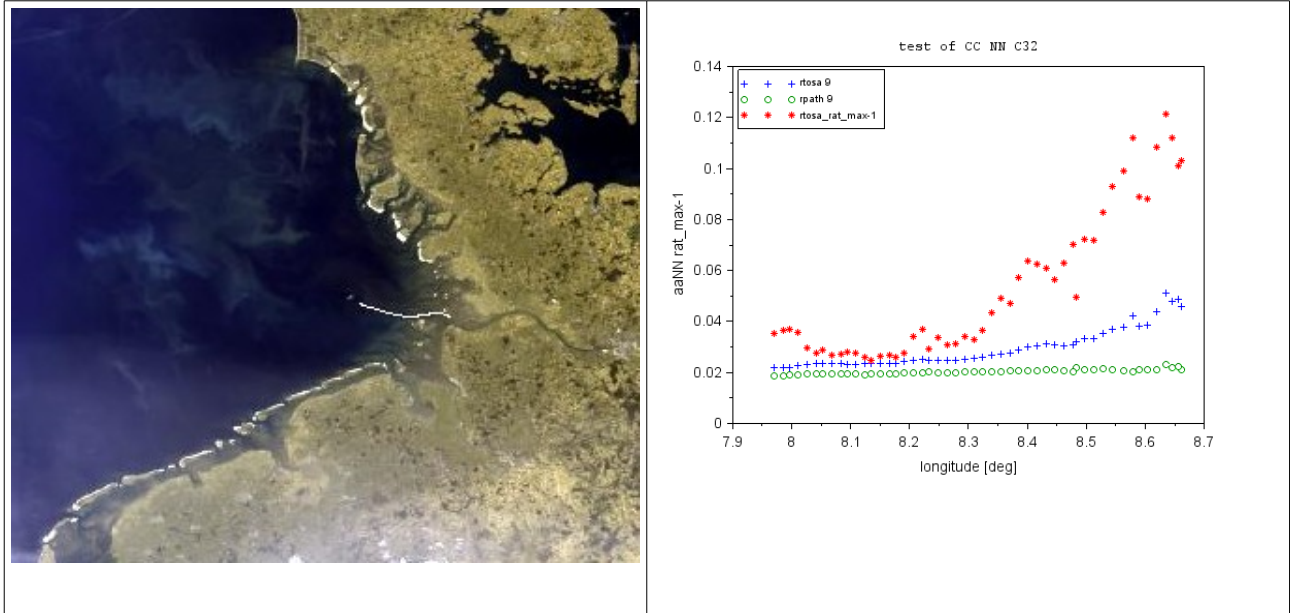


Fig. 46: Transect C32 (26.7.2006) between Cuxhaven and Helgoland with the track in the MERIS L1b scene of this day (left) and the reflectance along this track of Rtosa (blue) and the path radiance Rpath (green).

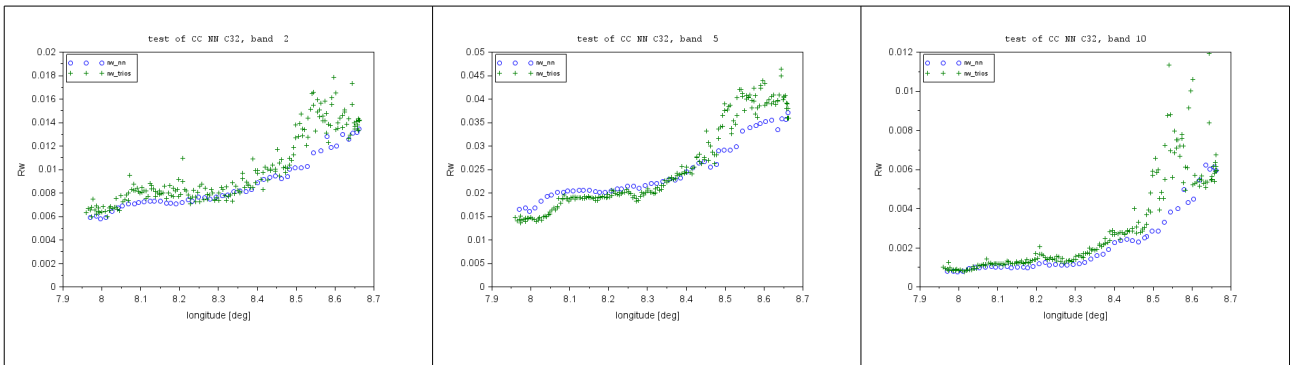


Fig. 47: Comparison of water leaving reflectances from MERIS and the TRIOS system.

	DOC:	MERIS Case 2 water ATBD 4 th reproc		
	DATE:	20150319		
	Issue:	2	Revision:	Page: 42 of 55

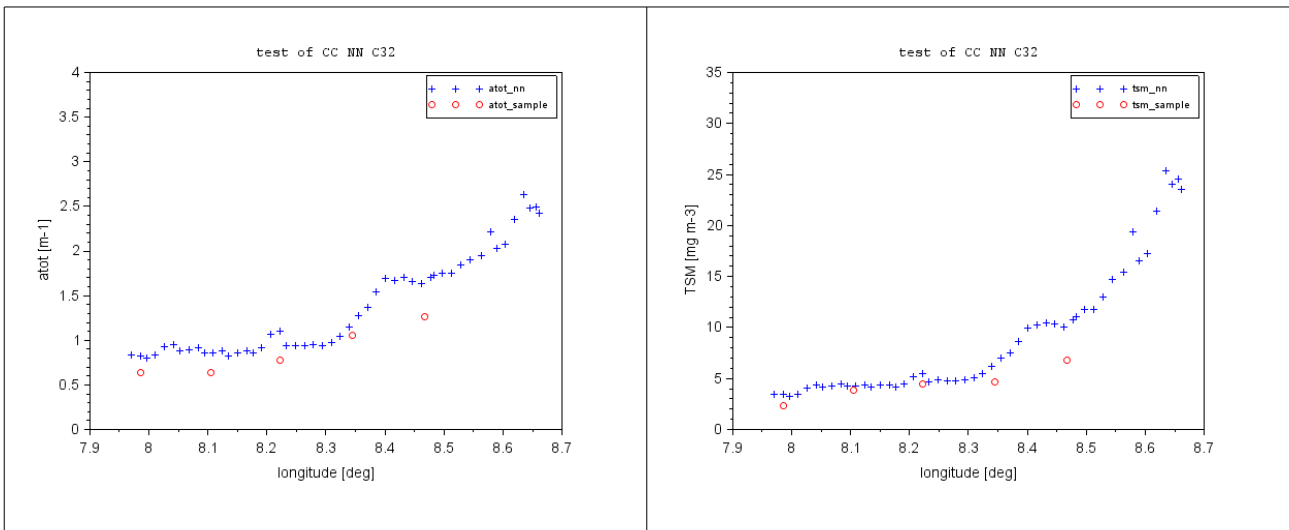


Fig. 48: Comparison between water samples (red) and MERIS data (blue) for the absorption coefficient (left) and total suspended matter dry weight (TSM) (right) of all water constituents.

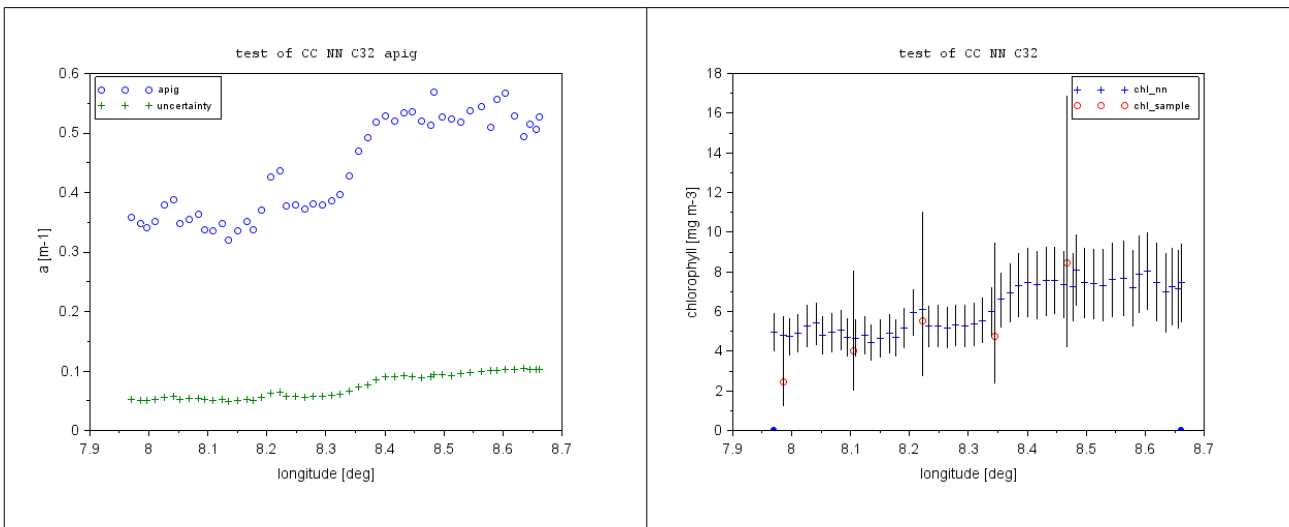


Fig. 49: Pigment absorption coefficient (left, blue) together with the uncertainty (green). On the right the corresponding chlorophyll concentration along the transect with the uncertainty range (vertical bars) and the chlorophyll concentration of the samples (red) with the factor 2 uncertainty range.

10.1.10 Summary and conclusions from Helgoland transects

The validation using the Helgoland transects do not show homogeneous results. Some MERIS data agree very well with the in situ observations, others are partly outside the factor 2 limit. Causes for inconsistent data are manifold in such coastal waters. The distribution of water constituents is very patchy with rapid changes due to tidal currents. Even the optical properties may change with the tidal current so that during high ebb and flood currents more heavier and coarser mineralic particles are raised to the surface than during calm high or low water phase. This, in particular, happens in the shallow coastal area and in the mouth of the estuary.

	DOC:	MERIS Case 2 water ATBD 4 th reproc		
	DATE:	20150319		
	Issue:	2	Revision:	Page: 43 of 55

The result of the aaNN gives the first hint if the further algorithms produce reliable results. Obvious is the high deviation in transect C18 (Büsum – Helgoland) at longitudes > 8.3 deg. (Fig. 14) This part of the transect is the Waddensea with very shallow water with partly dry fallen plains or contributions by bottom reflection. Obvious is the good separation of the path radiance reflectance from the tosa reflectance, which is presented for band 9 (708 nm). While in the clear water section longitudes < 8.1 deg the difference between R_{tosa} and R_{path} is very small, the difference increases towards the coast due to the contribution by the water reflectance in the area with high particle concentrations, which contribute to the reflectance even in the near infrared spectral region.

The deviation between R_{tosa} and the output of the aaNN is smaller in all other transects, i.e. the transects between the Elbe mouth and Helgoland, except for sections close to the estuary, where dry fallen plains but also heavy ship traffic with foam can be expected (e.g. see transect C28 – C32, Figs. 38, 42, 46), although the agreement between samples and MERIS data for total absorption and TSM is high (Figs. 40, 44, 48).

The comparison between the water leaving irradiance reflectances of MERIS and TRIOS shows an inhomogeneous picture in particular for the blue band at 443 nm, which is very sensitive to the correction of the skylight reflection in case of the TRIOS data. Since the reflectance of the water of this area is low due to the high concentrations of humic substances, small errors in the measurement of the sky radiance can lead to a relatively large error of the water leaving radiance. This is also true for the determination of R_w from MERIS data. Obvious e.g. is the large bias in the transect C18, which is nearly constant over the full transect. Furthermore, the scatter in the reflectances derived from TRIOS data is rather large and in the order of the deviation from MERIS R_w in some of the transects (C18, C23-C26).

The agreement of the total absorption coefficient at 443 nm ($a_{pig}+a_d+a_g$) and the total suspended matter concentrations (determined from the sum of b_p and b_w) between water samples and MERIS data is high in most transects (deviation < factor of 2). Even in transect C18, where the deviation in the water reflectance at 443 nm is highest.

For a_{pig} also the uncertainty in absolute units has been plotted (s. Fig. 17 For C18 and the following). It increases steadily towards the coast with increasing concentrations of the other water constituents. The corresponding chlorophyll concentration is shown on the right side of this figure. It shows both the factor 2 uncertainty range of the water samples as well as the uncertainties of the chlorophyll concentration derived from MERIS data. In most cases the MERIS data are within the factor 2 uncertainty range (= 30% on the log scale).

10.2 Validation using MERMAID data

The MERMAID data set (status of 2012) has been used to validate the atmospheric correction and the retrieval of chlorophyll.

10.2.1 Retrieval of R_w

For the test of the atmospheric correction 5 sites have been selected: Mediterranean Sea (AAOT), Pacific Ocean (MOBY), North Sea (Belgium Coast), Baltic Sea (Gustav Dalen Tower).

Fig. 50 shows the result for the AAOT data (Venice Tower, Adriatic Sea, Zibordi et al. xx). No data have been excluded due to flags. So also data with high sun glint are included. On the linear scale the slope of the regression deviates only by 1% from the 1by1 line. On the log scale the relatively

	DOC:	MERIS Case 2 water ATBD 4 th reproc		
	DATE:	20150319		
	Issue:	2	Revision:	Page: 44 of 55

lower values of the AAOT data in the low reflectance range reduces the slope to 0.925.

The relative scatter of the data on the log scale of 16% is within the acceptable range.

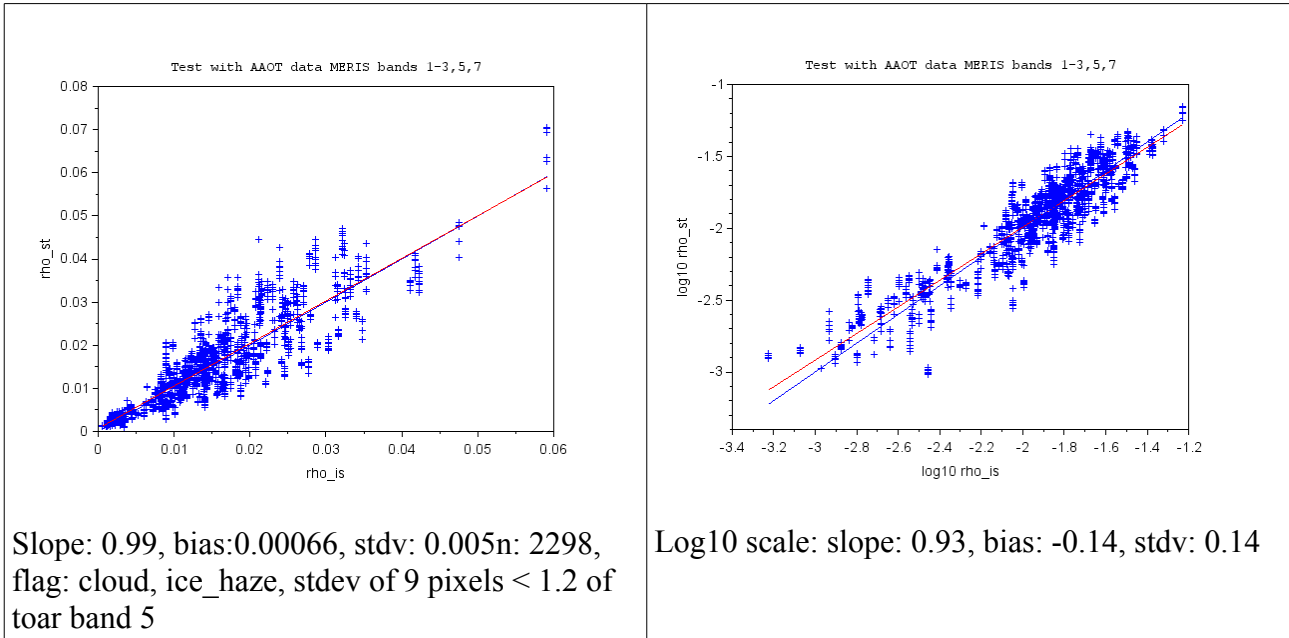
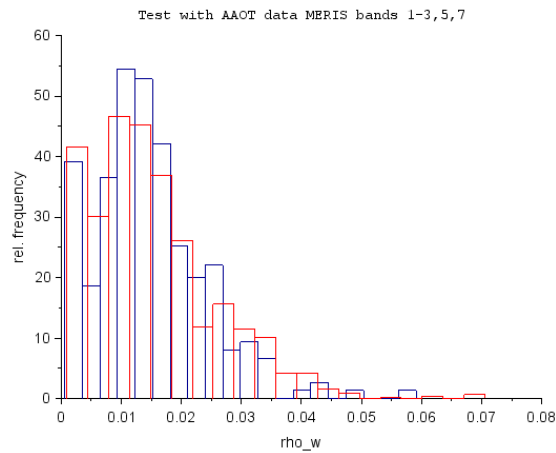


Fig. 50: Comparison of the water leaving irradiance reflectance with AAOT data for MERIS bands 1-3 and 5 and 7. 1by1 line blue, regression line red. Left on linear scale, right on log10 scale.



	DOC:	MERIS Case 2 water ATBD 4 th reproc		
	DATE:	20150319		
	Issue:	2	Revision:	Page: 45 of 55

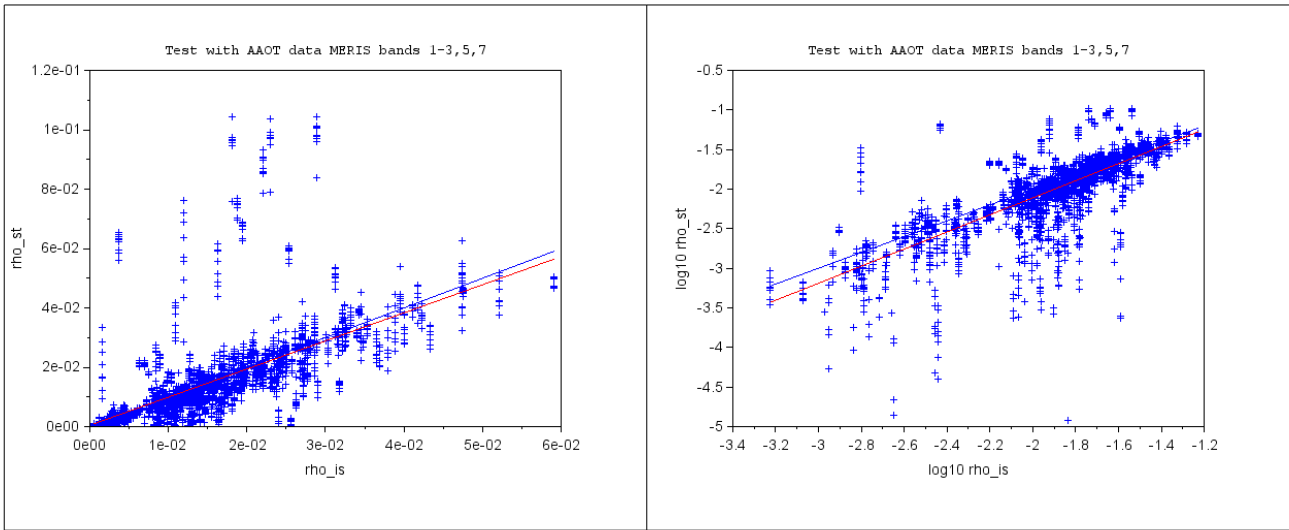


Fig. 52: Test of the standard atmospheric correction using the same AAOT data set. Left on linear, right on log scale

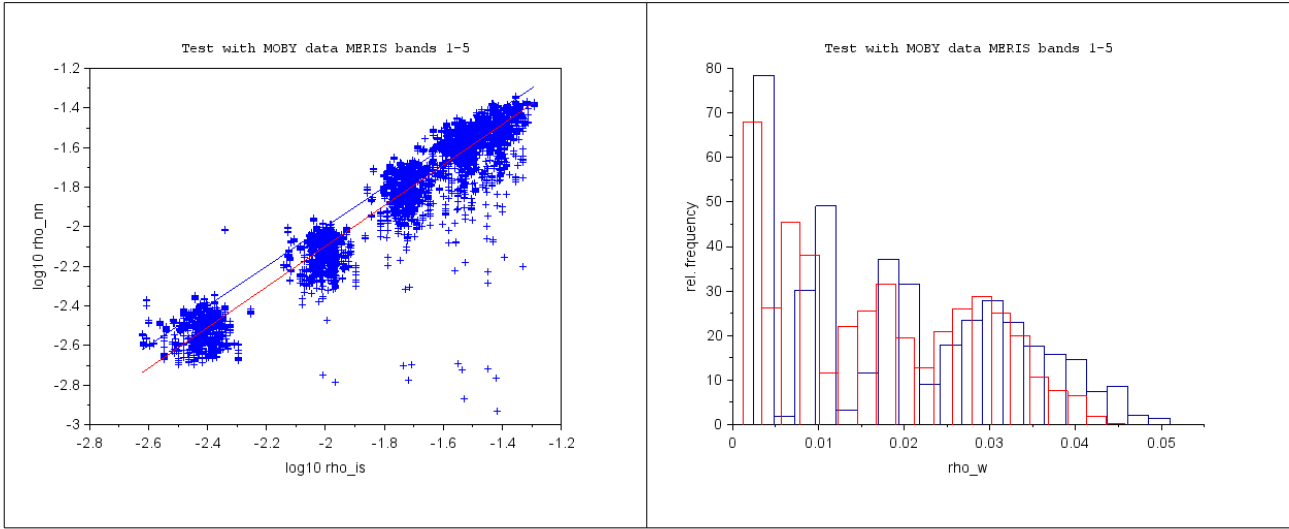


Fig. 53: Comparison of water leaving reflectance with MOBY data, left on log10 scale, right frequency distribution, blue MOBY data, red MERIS data

	DOC:	MERIS Case 2 water ATBD 4 th reproc		
	DATE:	20150319		
	Issue:	2	Revision:	Page: 46 of 55

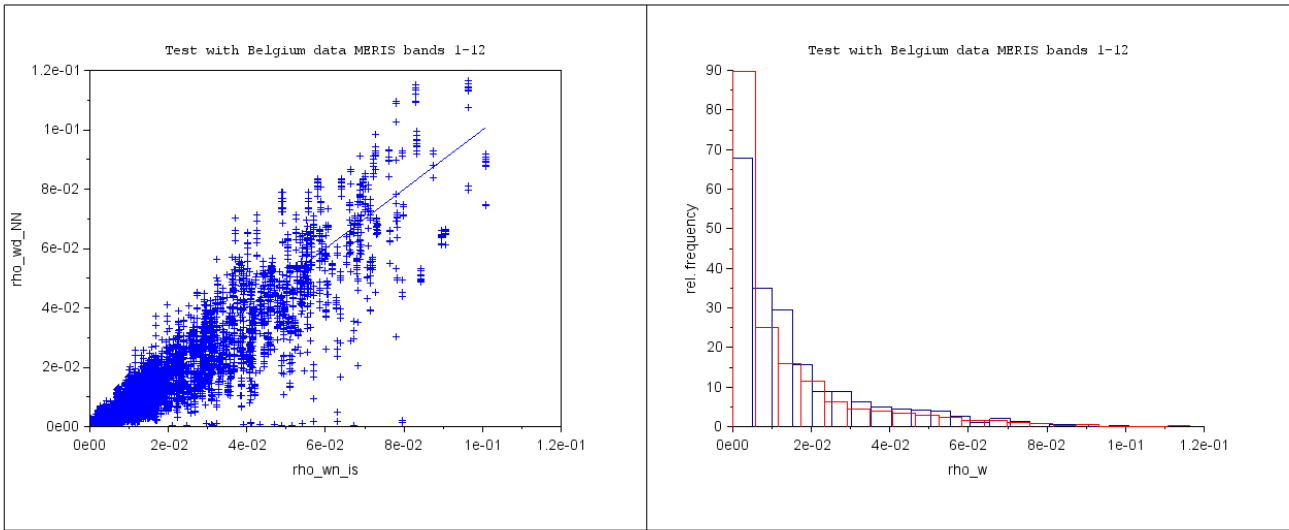


Fig. 54: Comparison of water leaving reflectance with data of the Belgium coast (K. Ruddick), left on linear scale, right frequency distribution, blue in situ data, red MERIS data

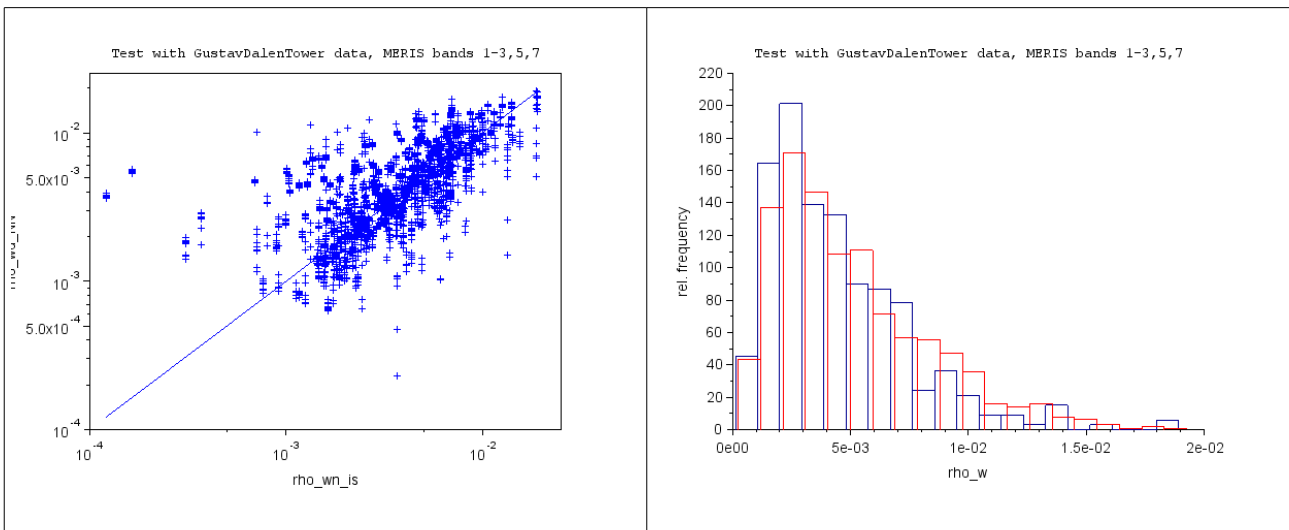


Fig. 55: Comparison of water leaving reflectance with data of the Baltic Sea, Gustav Dalen Tower (G. Zibordi), left on log scale, right frequency distribution, blue in situ data, red MERIS data

10.2.2 Validation of chlorophyll data

For the validation of the chlorophyll data two different MERMAID in situ data were used separately, which were measured using hplc (hplc_chla_total) with 514 samples (3x3 = 4626 pixels) and the fluorometric method (fluor_chla_is) with 239 samples (3x3 = 2637 MERIS pixel). As already indicated in the NOMAD data set, the fluorometric data has a lower scatter. The output of the NN, i.e. apig, was converted into chlorophyll a concentration by $\langle \text{chl_conc} \rangle = 20 * \text{apig}^{1.04}$.

The coefficient were derived from data of the North Sea by regression. As one can see in the following the coefficients, which were derived from regression with the MERMAID data set deviates from the coefficients, which were used up to now probably due to the fact that they are

	DOC:	MERIS Case 2 water ATBD 4 th reproc		
	DATE:	20150319		
	Issue:	2	Revision:	

more related to case 1 water.

The MERIS data were filtered using the following conditions: $windm < 8$ & $cloud < 1$ & $ice_haze < 1$ & $white_scatter < 1$.

10.2.3 Validation using HPLC total data

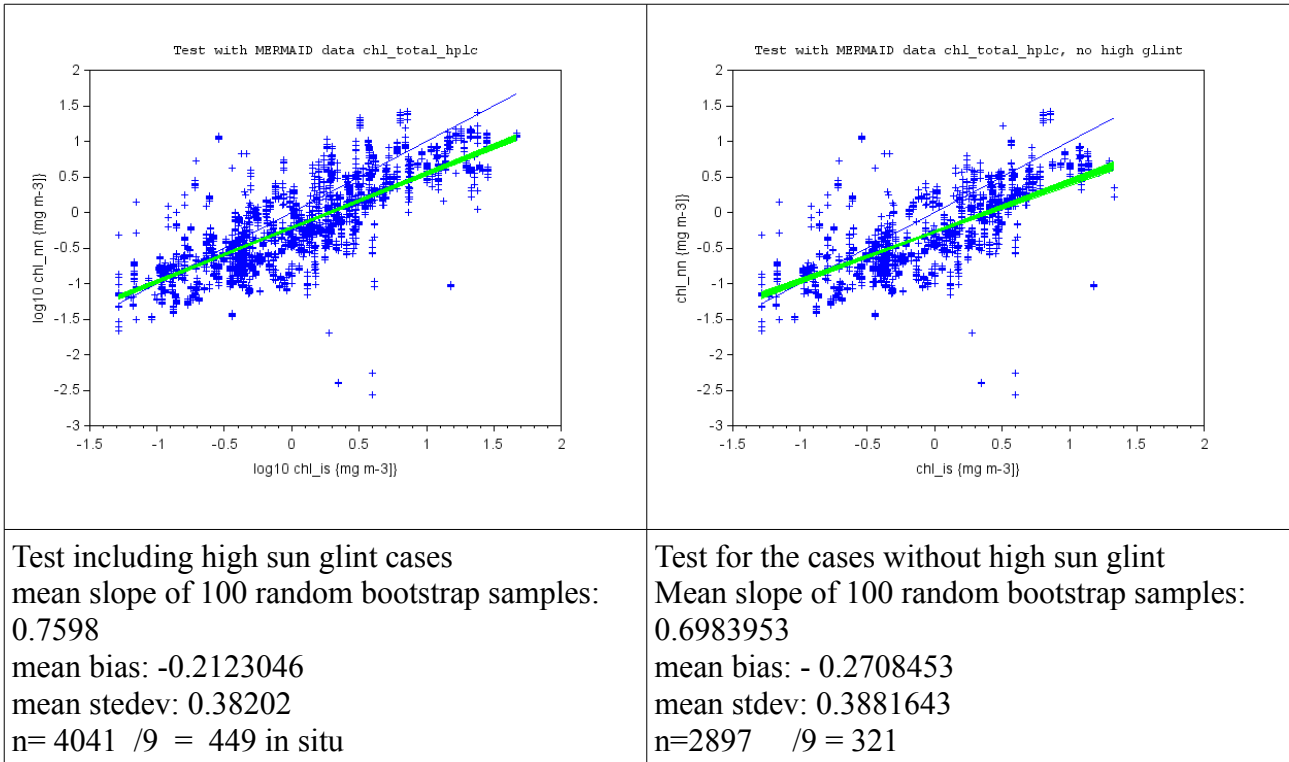


Fig. 56: Test using the hplc_total in situ data with and without high sun glint pixels

	DOC:	MERIS Case 2 water ATBD 4 th reproc		
	DATE:	20150319		
	Issue:	2	Revision:	Page: 48 of 55

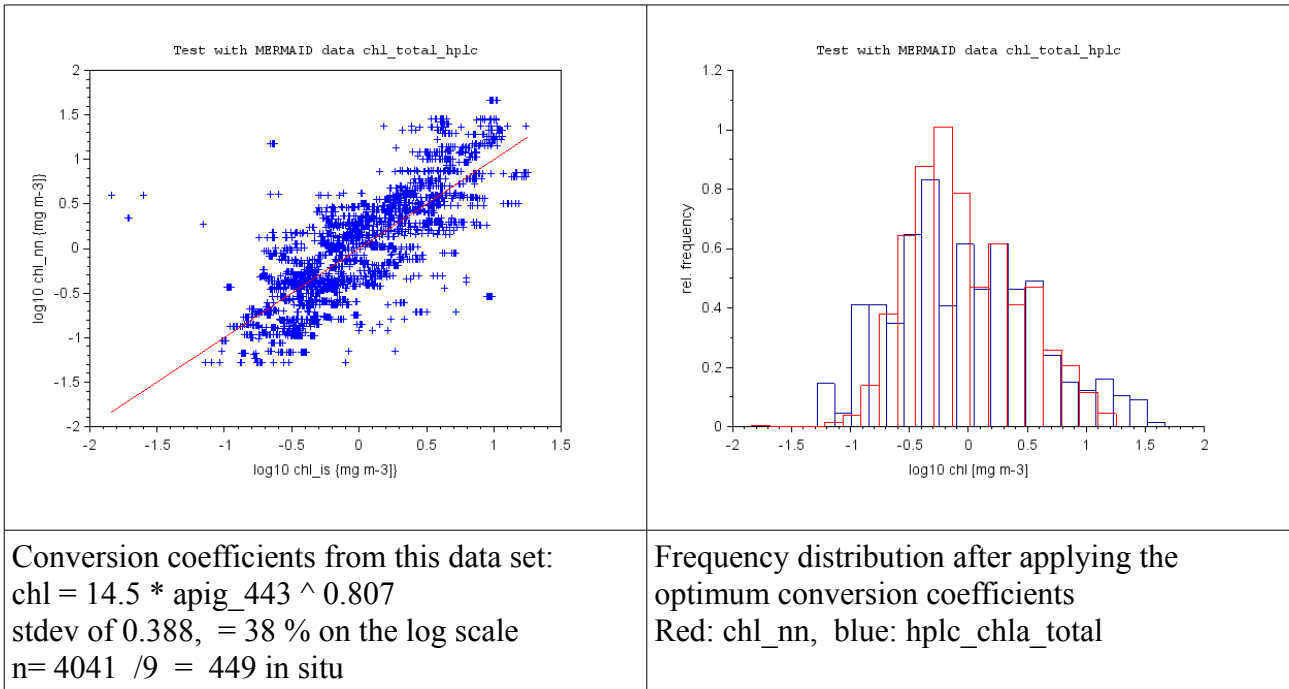


Fig. 57: Test after determining conversion coefficients from this data set

10.2.4 Test using the fluorometric chlorophyll data

This subset of chlorophyll data of MERMAID has been measured using the fluorometric method, which has a lower scatter. The standard deviation on the log scale is now 31% which corresponds to a factor 2 on the linear scale.

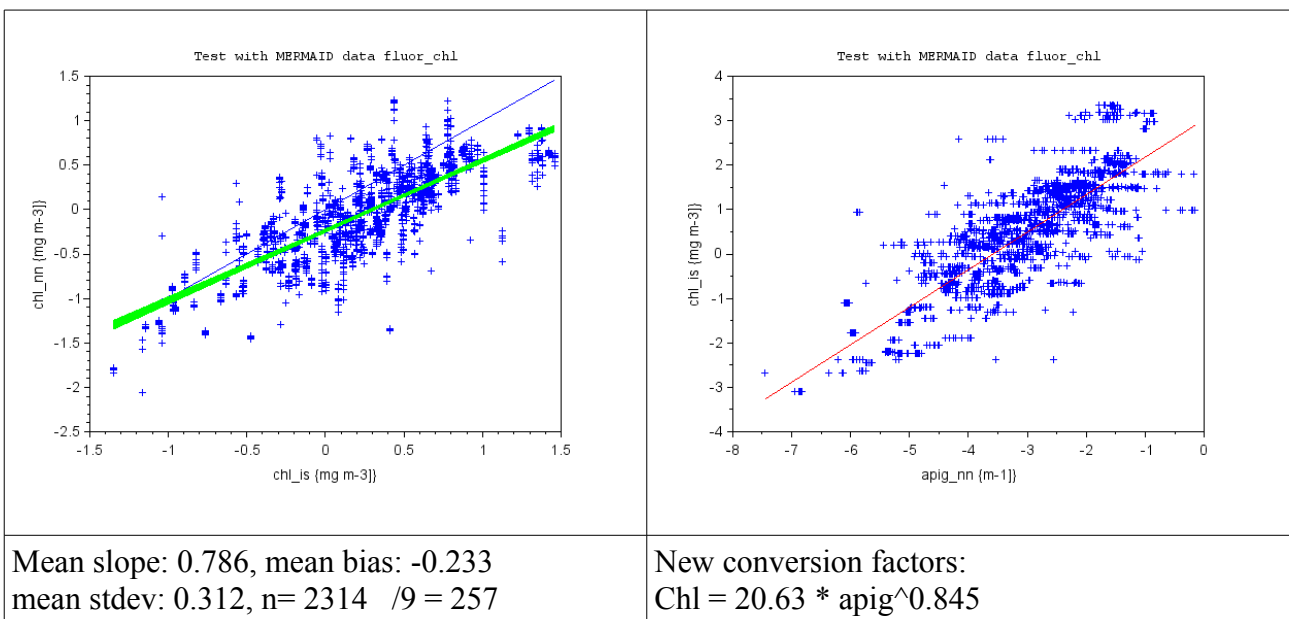


Fig. 58: Test using the fluorometric chlorophyll data of MERMAID. Left the test, right the relationship between apig and the chlorophyll concentration for the determination of new

	DOC:	MERIS Case 2 water ATBD 4 th reproc		
	DATE:	20150319		
	Issue:	2	Revision:	Page: 49 of 55

conversion coefficients

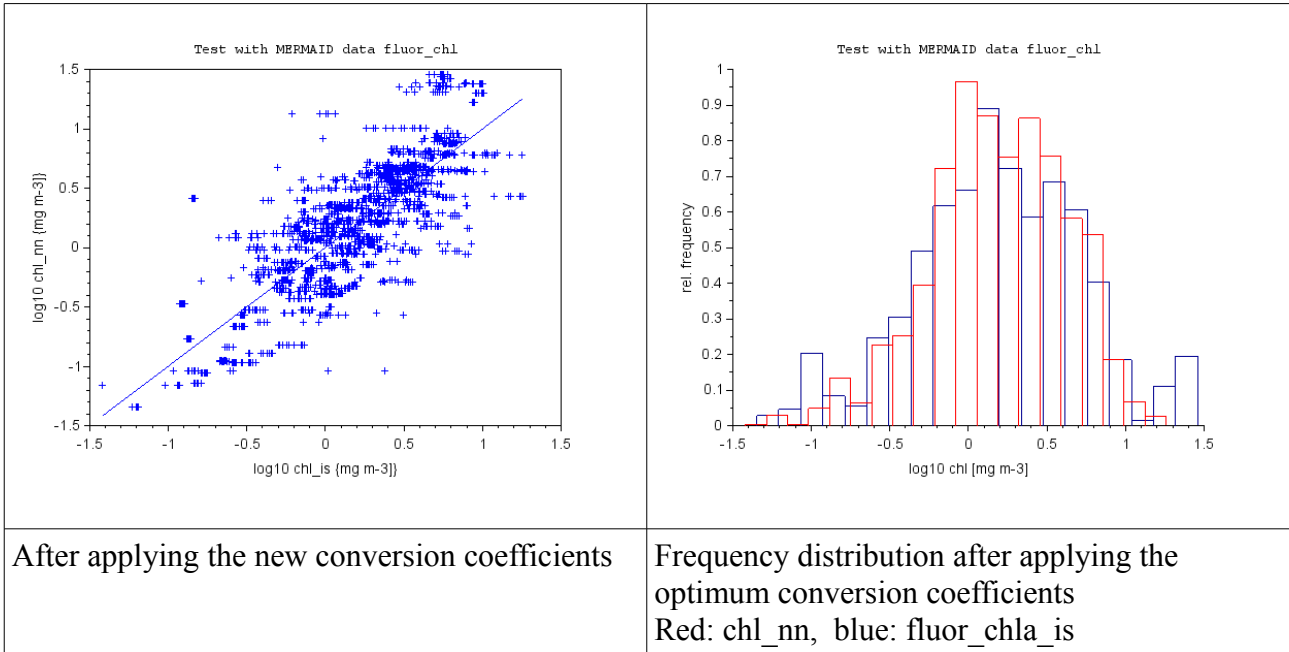


Fig. 59: The regression (left) and the frequency distribution (right) after using the new conversion coefficients

The conversion coefficients are different from those for the hplc chlorophyll concentrations. For comparison the conversion factors derived from the NOMAD data set (in situ data only) are provided in Fig. 60.

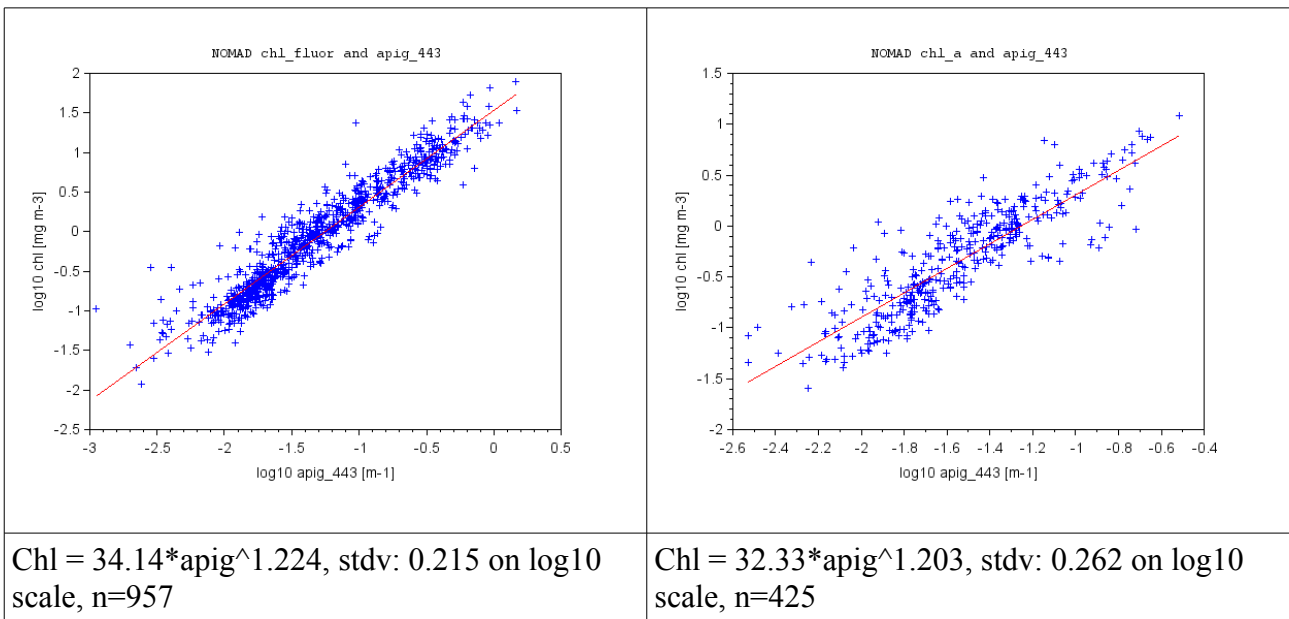


Fig. 60: Relationship between apig and chlorophyll concentration NOMAD data set, left for fluorometric and right for hplc data

	DOC:	MERIS Case 2 water ATBD 4 th reproc		
	DATE:	20150319		
	Issue:	2	Revision:	Page: 50 of 55

10.2.5 Summary and conclusions from the MERMAID test

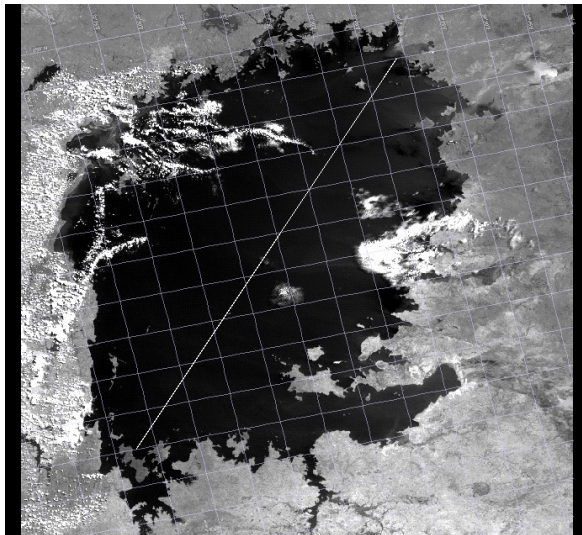
The comparison of Rw_{nn} with Rw_{is} from different sites of MERMAID shows an acceptable agreement with respect to slope and bias. The scatter of the data is larger than the desired 5% accuracy but with 16% on the log scale less than the results of the standard atmospheric correction procedure (30%, Fig. 52). Results which include data with high sun glint are within the same limits.

The chlorophyll concentrations have an uncertainty of 31% on the log scale, when compared to the fluorometric in situ data, which is within the desired factor of 2 range.

10.3 Test of the case 2 water procedure for high altitude inland waters

This test has been performed to verify the applicability of the NN with pressure input to lakes in high altitudes. It was applied to a MERIS scene of Lake Victoria in East Africa, which is located in an altitude of 1134 m. The pressure in this altitude was computed with the simple formulation, which will later be replaced in MEGS with a more accurate version:

```
tosa_press=atm_press*exp(-1134.0/8000); // only for lake victoria
```



Transect Lake Victoria (East Africa)

MERIS L1b FR 20050903

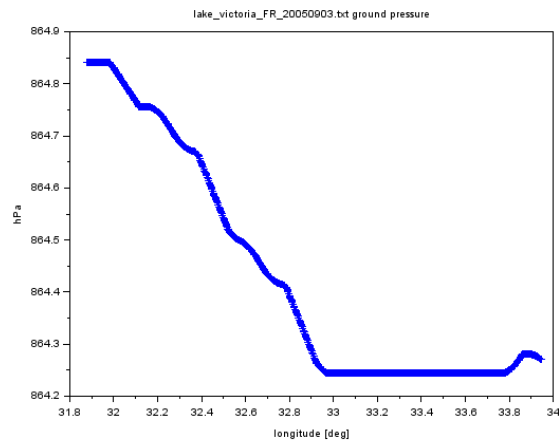
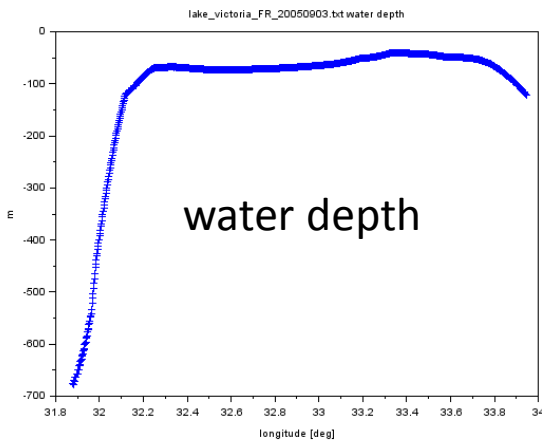


Fig. 61: MERIS FR scene of Lake Victoria, 20050903 (above), with water depth and surface

	DOC:	MERIS Case 2 water ATBD 4 th reproc		
	DATE:	20150319		
	Issue:	2	Revision:	Page: 51 of 55

pressure along transect.

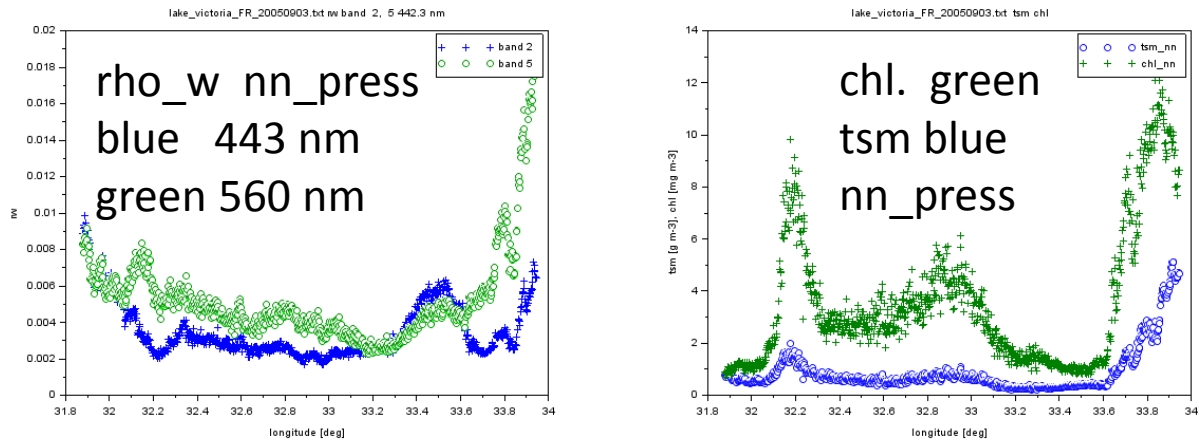


Fig. 62: water reflectance along transect (left), blue for 443 nm, green for 560 n; right chlorophyll and TSM concentration along transect, determined with the NN algorithm.

10.4 Sun glint and high reflectance test

The applicability of the algorithms to scenes with sun glint has been verified with a MERIS scene of the Northwest Atlantic Ocean. Fig. 63 Shows the high reflectance due to sun glint area along the transect at 865 nm (b), while after the AC the water reflectance (d) does not show any impact of sun glint. Of interest is also the counter-rotating reflectance of MERIS and 2 (443 nm) and 5 (560 nm) along the transect, when different types of water masses are encountered.

	DOC:	MERIS Case 2 water ATBD 4 th reproc		
	DATE:	20150319		
	Issue:	2	Revision:	Page: 52 of 55

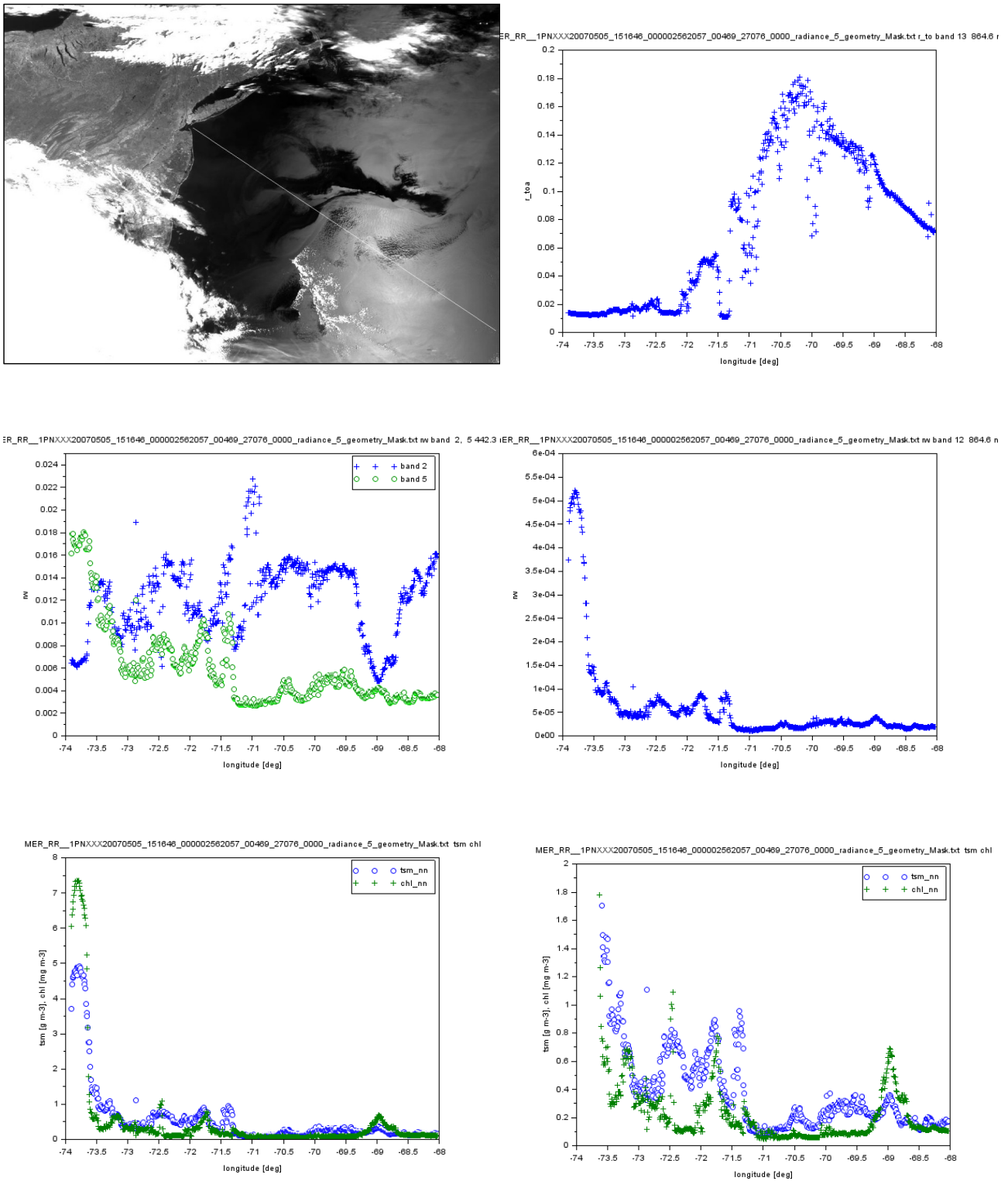


Fig. 63: MERIS scene of the Northwest Atlantic with sun glint and transect; (b) TOA reflectance at 865 nm, (c) water reflectance at 443 and 560 nm, (d) water reflectance at 865 nm, (e) TSM (blue) and chlorophyll (green) along transect, (f) as e but with higher resolution for resolving the lower concentration range.

	DOC:	MERIS Case 2 water ATBD 4 th reproc		
	DATE:	20150319		
	Issue:	2	Revision:	
				Page: 53 of 55

11 Summary and Conclusions

The proposed system of case 2 water algorithms for the 4th reprocessing is based on the results of Coastcolour. It includes a procedure to compute reflectance spectra at top of a standard atmosphere (Rtosa) with a surface pressure of 1013.2 hPa and a non absorbing atmosphere, a neural network to detect out of scope spectra, neural networks to determine water leaving reflectance, path radiance reflectances and the absorption and scattering coefficients of 5 water components and a NN to determine the uncertainties of these 5 components.

Compared to the previous versions it includes the following major changes:

- a new bio-optical model, which is based on NOMAD and Coastcolour data with respect to
 - optical properties of 5 components
 - concentration ranges
 - frequency distribution
 - co-variances
- uncertainties for training of the NN
- model of the atmosphere, which is based on coastal AERONET stations
- aaNN for detecting L1b spectra, which are out of scope
- NNs for determining the uncertainties of the derived IOPs

The validation using data of the Helgoland transect and of MERMAID indicate an improvement with respect to the previous version. Most results are within the desired limits, which is a standard deviation of 30% on the log scale when compared to in situ samples.

The procedure for determining the water reflectance produces results, which are in the same range or better when compared to the standard atmospheric correction and works also under high sun glint conditions.

12 Acronyms

Tbc

Acronym, Symbol	alternative	Explanation
a_ozone		Absorption coefficient of ozone
aaNN		Auto-associative neural network
ad		Absorption coefficient of detritus at 443 nm
adg		Absorption coefficient of detritus + gelbstoff
ag		Absorption coefficient of gelbstoff at 443 nm
apig		Absorption coefficient of phytoplankton pigments at 443 nm
Bb		Backscattering factor

	DOC:	MERIS Case 2 water ATBD 4 th reproc		
	DATE:	20150319		
	Issue:	2	Revision:	
Page: 54 of 55				

Acronym, Symbol	alternative	Explanation
bbp		Particle backscattering coefficient
bp		Scattering coefficient of particles at 443 nm
btsm		Scattering coefficient of particles and white particles = total suspended matter
bw		Scattering coefficient of white particles at 443 nm
c_ozone		Concentration of ozone in dobson units (DU)
Edtosa		Downwelling irradiance at top of standard atmosphere
ex_ad		Spectral exponent of detritus absorption spectrum
ex_ag		Spectral exponent of gelbstoff absorption spectrum
ex_bp		Spectral exponent of particle scattering spectrum
ex_bw		Spectral exponent of white particle scattering spectrum
h2o_corpoly		Polynomial for the correction of water vapour
hPa		Hecto Pascal, pressure unit
IOP		Inherent Optical Property, e.g. absorption and scattering
IOPforNN		NN with IOPs as input and Rw as output
IOPinvNN		NN with Rw as input and IOPs as output
log10		Decadal logarithm
logn		Natural logarithm
Ltosa		Radiance at top of standard atmosphere
MERIS		Medium Resolution Imaging Spectrometer
NN		Neural Network
NOMAD		
rand		Random number
RL		Radiance reflectance
Rpath		Path radiance reflectance, which includes the Fresnel reflection at the water surface
RpathNN		NN with rtosa as input and Rpath as output
Rtoa		Reflectance at top of atmosphere
Rtosa		Reflectance at top of standard atmosphere (1013.2 hPa, no ozone)
Rtosa_h20		Reflectance at TOSA, corrected for the influence of ozone
Rtosa_h20_ozone		Reflectance at TOSA, corrected for the influence of water vapour and ozone

	DOC:	MERIS Case 2 water ATBD 4 th reproc		
	DATE:	20150319		
	Issue:	2	Revision:	
				Page: 55 of 55

Acronym, Symbol	alternative	Explanation
Rw		Water leaving irradiance reflectance
Rwf		Apparent water leaving reflectance due to solar stimulated fluorescence of phytoplankton
RwNN		NN with R _{tosa} as input and Rw as output
s		
solflux		Solar flux at TOA
TOA		Top of Atmosphere
TOSA		Top of Standard Atmosphere
trans_ozone		Transmittance of the total ozone
uncNN		Uncertainty NN for IOPs
θ_s		Sun zenith angle
θ_v		Viewing zenith angle
λ		wavelength
φ		Azimuth difference sun - viewing

13 References

Tbc

AZNAY O. AND R. SANTER (2009) MERIS atmospheric correction over coastal waters: Validation of the MERIS aerosol models using AERONET. International Journal of Remote Sensing, 30(18), pp. 4663 - 4684. DOI: 10.1080/01431160802632256

LENOBLE J., M. HERMAN, J.L. DEUZE,, B. LAFRANCE, R. SANTER, D. TANRE ,. (2007). A successive order of scattering code for solving the vector equation of transfer in the earths atmosphere with aerosols Journal of Quantitative Spectroscopy & Radiative Transfer 107 (2007) 479507

ZAGOLSKI R., SANTER R., AZNAY O., (2007). A new climatology for atmospheric correction based on the aerosol inherent optical properties. Journal of Geophysical Research, Vol. 112, No. D14, D14208